Comparison of Ballistic Responses of Different Types High Hardness Perforated Armor Plates Against Armor Piercing Projectiles

Author

BILAL IBRAHIM

Regn Number

FALL2017-MSDME-0000205903

Supervisor

Dr. Aamir Mubashar

DEPARTMENT OF DESIGN AND MANUFACUTRING ENGINEERING

SCHOOL OF MECHANICAL & MANUFACTURING ENGINEERING

NATIONAL UNIVERSITY OF SCIENCES AND TECHNOLOGY

ISLAMABAD

SEPTEMBER 2020

Comparison of Ballistic Responses of Different Types High Hardness Perforated Armor Plates Against Armor Piercing Projectiles

Author

BILAL IBRAHIM

Regn Number

FALL2017-MSDME-0000205903

A thesis submitted in partial fulfillment of the requirements for the degree of

MS Design and Manufacturing Engineering

Thesis Supervisor:

Dr. Aamir Mubashar

Thesis Supervisor's Signature: _____

DEPARTMENT OF DESIGN AND MANUFACUTRING ENGINEERING

SCHOOL OF MECHANICAL & MANUFACTURING ENGINEERING

NATIONAL UNIVERSITY OF SCIENCES AND TECHNOLOGY,

ISLAMABAD

SEPTEMBER 2020

Declaration

I certify that this research work titled "*Comparison of Ballistic Responses of Different Types High Hardness Perforated Armor Plates Against Armor Piercing Projectiles"* is my own work. The work has not been presented elsewhere for assessment. The material that has been used from other sources it has been properly acknowledged / referred.

Signature of Student

BILAL IBRAHIM

FALL2017-MSDME-0000205903

Plagiarism Certificate (Turnitin Report)

This thesis has been checked for Plagiarism. Turnitin report endorsed by Supervisor is attached.

Signature of Student

BILAL IBRAHIM

Registration Number

FALL2017-MSDME-0000205903

Signature of Supervisor

Copyright Statement

- Copyright in text of this thesis rests with the student author. Copies (by any process) either in full, or of extracts, may be made only in accordance with instructions given by the author and lodged in the Library of NUST School of Mechanical & Manufacturing Engineering (SMME). Details may be obtained by the Librarian. This page must form part of any such copies made. Further copies (by any process) may not be made without the permission (in writing) of the author.
- The ownership of any intellectual property rights which may be described in this thesis is vested in NUST School of Mechanical & Manufacturing Engineering, subject to any prior agreement to the contrary, and may not be made available for use by third parties without the written permission of the SMME, which will prescribe the terms and conditions of any such agreement.
- Further information on the conditions under which disclosures and exploitation may take place is available from the Library of NUST School of Mechanical & Manufacturing Engineering, Islamabad.

Acknowledgements

First of all, I am thankful to my Creator Allah Almighty who guided me throughout this work at every phase.

I would also like to express special thanks to my supervisor Dr. Aamir Mubashar for his continuous help, expert guidance and strong support throughout my thesis. I would also like to pay special thanks to Brigadier Dr. Syed Waheed Ul Haq for his tremendous support and cooperation during experimentation.

Finally, I would like to express my gratitude to all the individuals who have rendered valuable assistance to my study.

Dedicated to my parents

Abstract

A comparison has been drawn on ballistic responses of different types of perforation in high hardness armor plates against armor piercing projectiles through experimentation in the research. The ballistic response of an aluminum base armor plate and a combination of different types of high hardness perforated armor plates and aluminum base armor plate were determined against 7.62 mm armor piercing projectile. Three different perforations were made in high hardness perforated steel plates i.e., circular, diamond and slot perforations. The base armor plate alone was not able to stop projectile and it penetrated throughout. While when the same base armor high hardness perforated armor plates, projectile was stopped. Depressions were formed on the surface of the base armor plate from the impact of the projectile fragments. Video of impacts were also recorded through high speed camera.

Key Words: *Perforated Armor, Armor Piercing Projectile, Ballistic Response*

Table of Contents

List of Figures

List of Tables

CHAPTER 1: INTRODUCTION

In this dissertation, the research work has been divided into two phases. First phase deals with experimentation of multi layered armor plates against armor piercing projectiles while second part deals with the analysis run in Abaqus CAE Software to validate these experiments.

1.1 Background

For applications pertaining to combats and warfare, resistance to impact penetration and resilience ability to shock are very vital. Study of response of armor materials to shock and impact play dynamic role in developing improved armor for civilian and military applications. The designing, development and manufacturing of bullet proof materials involve study of response of materials under consideration so that their shock resilience can be enhanced. Weapon and bullets are being improved from time to time, which require improvement in protection against newly developed threats.

Pakistan has been fighting against terrorism since last two decades and has eliminated it to a greater extent. But still many security threats prevail. To increase protection armored vehicles and guard posts, security forces are in search of different ways to protect their civilians and military personnel safe from threats especially small calibers. Usage of armor systems is one of the primary and efficient defense approaches being deployed. But even most effective armored vehicles have been compromised which indicated requirement for development of better alternative materials for upgraded protection. High strength armored plates are usually used for protection of personnel in armored vehicles which cause increase in weight and difficulty in mobility. Also, such plates characteristically fail due to softening of material by strong agglomeration of plastic deformation undergoing major adiabatic heat in few shear planes. Tougher materials, similar to ceramics don't have ample toughness and generally require to be layered by more ductile materials for protection. The objective of our research is to study and evaluate armor systems containing hardened steel. High strength armor steel is anticipated to fortify metal matrixes, scatter plastic deformation and halt creation of adiabatic shear bands. The requirements for designing an armor protection need the application of that particular protection system. The essential aspects of a protection system include its cost, protection capability, weight and mobility. Different research scholars analyzed the ballistic response and performance of metals, polymers, ceramics and their composites. Even

with availability of numerical and experimental models on impact penetration and perforation of different projectiles on ductile materials including metals and ceramics, only limited research has been carried out to study damage evolution and criteria pertaining to failure in high hardness perforated armor steel when impacted with hardened steel core projectile.

Impact loading, damage and deformation in armored materials is usually studied experimentally. But experiments are costly, require much time and multiple test prototypes, calibrated equipment and precise settings. Using Finite Element Analysis (FEA) technique, a comprehensive primary study can be performed in a simulated medium through a computer-generated model. This can reduce cost, lessen the required time and significantly augment the general development process for materials used in armoring. The goal of research is to employ FEA technique using Abaqus CAE software for modelling the impact of armor piercing projectiles on different types of high hardness perforated plates.

During last three to four decades, many scholars have been trying to interpret behavior of high velocity impact by studying the high strain rate response of different materials. Research scholars have been deploying new methods and programs with advancement of technology. The newly developed numerical analysis methods are providing a more accurate and closer to reality picture of impact response to the researchers. Numerical analysis methods also save enormous experimental cost which would have incurred. This research also presents similar study concerning ballistic response of high hardness perforated armor steel plates.

High hardness perforated armor steel of different patterns and arrangements is being used by defence industry of whole world. These high hardness perforated armor steel plates have a consistent pattern of holes and perforations which are specially designed. In 1986, Ben-Moshe developed high hardness perforated steel armor for armored personnel carriers [1]. The design of holes must be in such a way that its diameter must be lesser than the diameter of caliber, it is designed to defeat. Triangle shaped perforations on high hardness armor steel plate were developed by Auyer et al in 1991 [2]. Ravid and Hirschberg introduced an armor system for defeating small calibers having a secondary perforated plate with 40~50% area covered with perforations [3]. Smith and Norris improved design of slot shaped perforations thus reducing weight up to 50% than solid plate [4]. Experimental as well as numerical analysis on high hardness perforated armor steel plates were carried out by Kılıç et al. to examine bullet defeating mechanism [5].

1.2 Objective

The primary emphasis of this research is to explore response of high hardness perforated armor steel plate having different types of perforations when impacted with high velocity projectile through experiments and finite element analysis techniques. The goals of this research are as under:

1. To investigate the reaction of different high hardness perforated armor steel plates against armor piercing projectile cores.
2. To use Finite Element Analysis to predict behavior of high hardness perforated armor steel plates against armor piercing projectiles.
3. To evaluate the failure mechanism happened on projectile cores and high hardness perforated armor steel plates after the impact.
4. To determine possible benefits of high hardness perforated armor steel plates.
5. To determine the result of different perforations on impact and shock resistance of high hardness perforated armor steel plates.
6. To validate the Finite Element Analysis simulation models of ballistic impacts on high hardness perforated armor steel plates and aluminum armor by employing the data available in literature.

1.3 Research Methodology

Before development and manufacturing of prototype high hardness perforated armor steel plates, Finite Element Analysis Techniques may be used to reduce overall cost incurring in experimentation. But due to extensive and vast research field of numerical analysis in CAE, a base is required. Detailed literature review is required to initiate computational ballistics. Figure 1.1 depicts research methodology for relevant field of research in form of a flow diagram.

Finite Element Analysis result and model of materials will be validated by applying outcomes of ballistic experimentation. The primary focus of this research is “Numerical Analysis”. The “Ballistic Experimentation” and “Finite Element Analysis Techniques” have been used for endorsement and characterization of material properties and parameters. Abaqus CAE software will be used for implementation of finite element technique for numerical analysis.

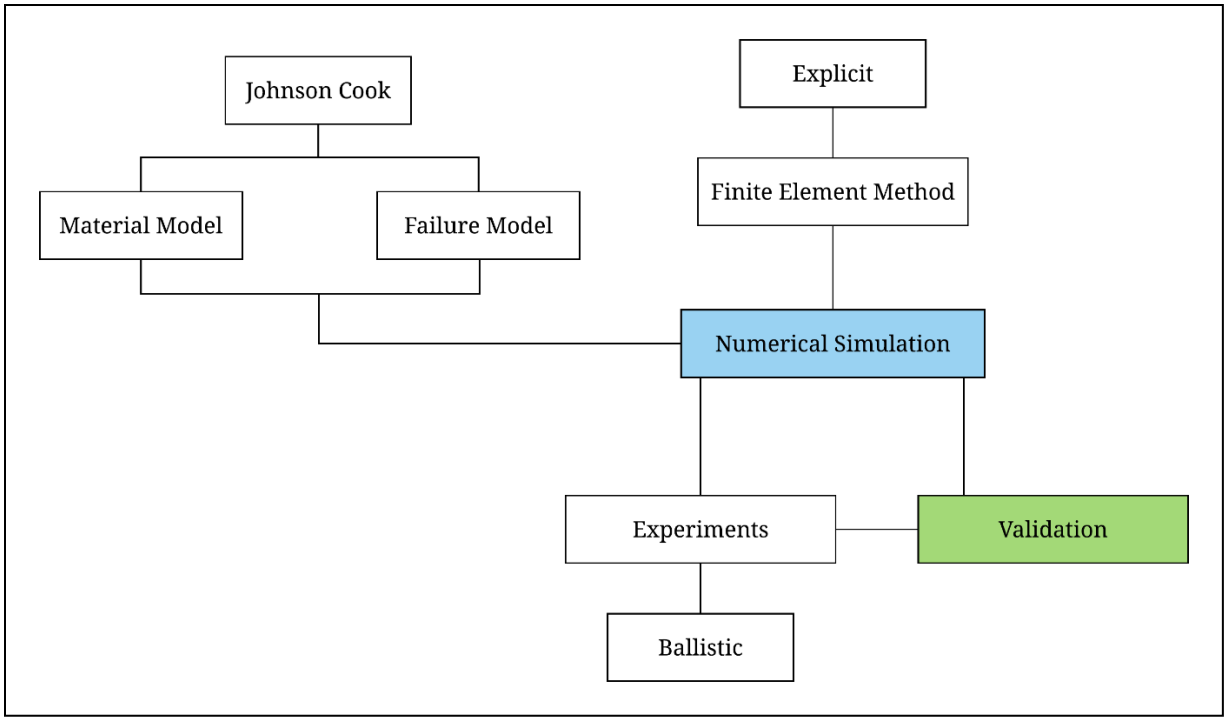

Figure 1.1: Research Methodology

CHAPTER 2: LITERATURE REVIEW

2.1 Deformation in Metals

A metal undergoes elastic and partially plastic deformation when sufficient load is applied. Deformation level usually depends upon the applied load, properties of material, its size and geometry. Figure 2.1 depicts conventional stress and strain graph for a ductile metal such as aluminum or steel. Additionally, high temperature rise, softening and extensive plastic deformation or sometimes failure can be seen in strain rate dependent high velocity impact scenarios because heat energy generated in result of friction and plastic deformation has no time to spread or disperse.

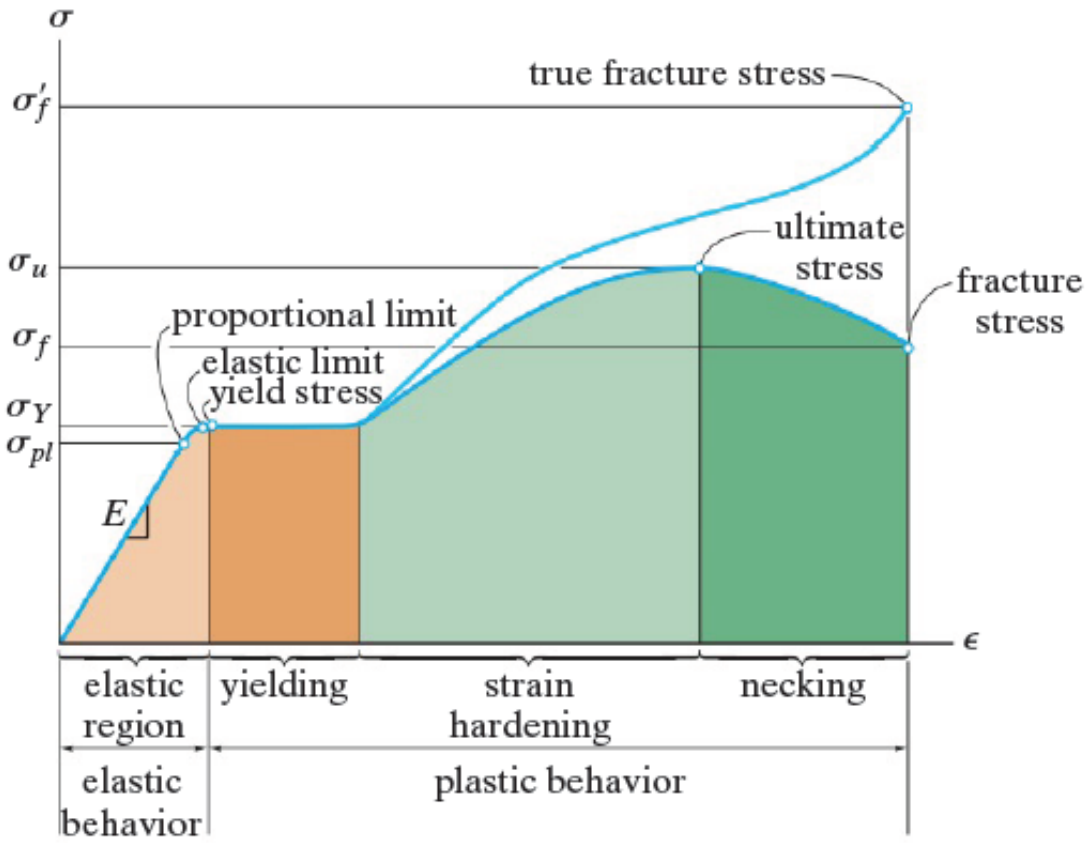

Figure 2.1: Conventional Stress and Strain Graph for a Ductile Metal [6]

2.1.1 Elastic Deformation

Elastic deformation of material is governed by Hooke's Law. In this region, linear behavior is shown by stress and strain graph and material returns to its original size upon removing of load [7]. Hooke's law is only applicable to materials which deform linearly in elastic region.

$$\sigma = E.\varepsilon \tag{1}$$

Where σ is stress applied, E is Young's Modulus and ε is the induced strain. This relationship allows the determination of modulus of elasticity. Modulus of elasticity is calculated as slope of stress and strain graph in elastic region. Elastic regions end at yield strength. After yield strength, material starts deforming plastically as shown in figure 2.1.

2.1.2 Plastic Deformation

As soon as material reaches its yield strength, plastic deformation starts which is permanent. Hooke's law is not valid in plastic region because strain induced is not proportional to stress applied in this region. In stress and strain graph, plastic region comprises of yielding, strain hardening, necking ang then fracture of material. After yielding regions ends, material will support increase in stress due to any load, ensuing a continuous rising curve which becomes flatter upon reaching ultimate stress. This upsurge in curve is called strain hardening [6]. After ultimate strength point, material starts localized elongation and strain becomes concentrated at a small section of the material. Area of this cross section starts reducing significantly, identified as necking till fracture happens. The stress calculate just before the fracture is called fracture stress [7].

Classification of failure of a material as ductile or brittle depends upon its ability to undergo plastic deformation before fracture. Ductile materials have elastic behavior, yielding, plastic deformation, strain hardening and necking as deformation stages. While brittle materials have slight or no yielding, instead they fail suddenly on minute plastic deformation. The reduction in area and elongation can be expressed through following formulas [8]:

$$\%\ \text{reduction in area} = \left(A_o - \frac{A_f}{A_o}\right) \times 100 \tag{2}$$

$$\%\ \text{elongation} = \left(l_f - \frac{l_o}{l_f}\right) \times 100 \tag{3}$$

Where A_o and l_o are initial area of cross section and initial length of the material while A_f and l_f are final area of cross section and length of material after failure.

2.1.3 Energy of Deformation and Fracture

When an external force distorts a material, strain energy is stored in complete volume of that material [6]. Strain energy stored per unit volume (u) of material is known as strain energy density and is expressed by following expression:

$$u = \frac{1}{2}\sigma\varepsilon \tag{4}$$

The ability of material to absorb energy while in its elastic region is known as resilience. The energy absorbed by unit volume of material within elastic range is called Modulus of Resilience (u_r) [9]. Area under stress and strain graph till elastic limit represents modulus of resilience (Figure 2.2).

$$u_r = \frac{1}{2}\frac{\sigma_{pl}^2}{E} \tag{5}$$

Where σ_{pl} is stress under elastic limit and E is Young's modulus of the material.

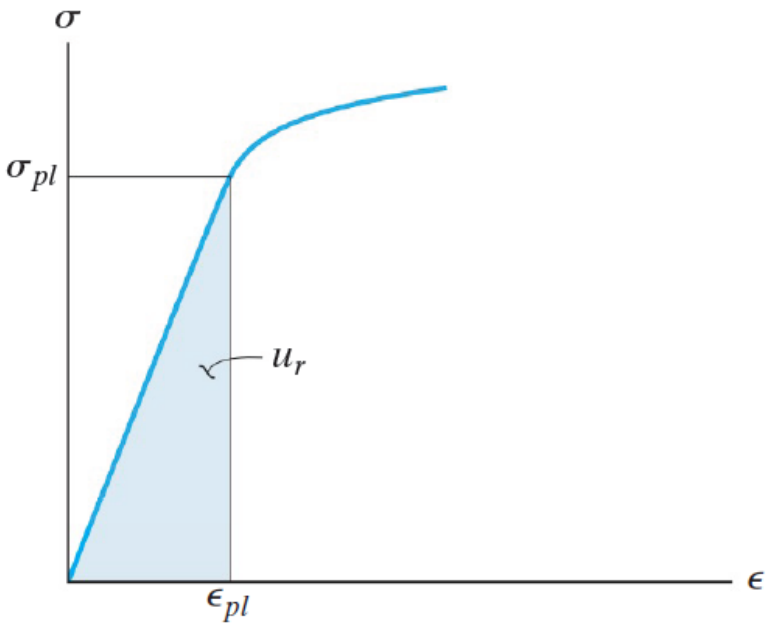

Figure 2.2: Modulus of Resilience from Stress-Strain Graph [6]

Toughness is ability of a material to absorb energy without failure. Energy absorbed in a unit volume of a material is known as Modulus of Toughness (u_T) [9]. Modulus of toughness is

represented by total area under stress and strain graph till fracture or failure point (Figure 2.3). It can also be expressed as:

$$u_T = \int_0^{\varepsilon_f} \sigma . d\varepsilon \quad (6)$$

Where ε_f is strain at failure point.

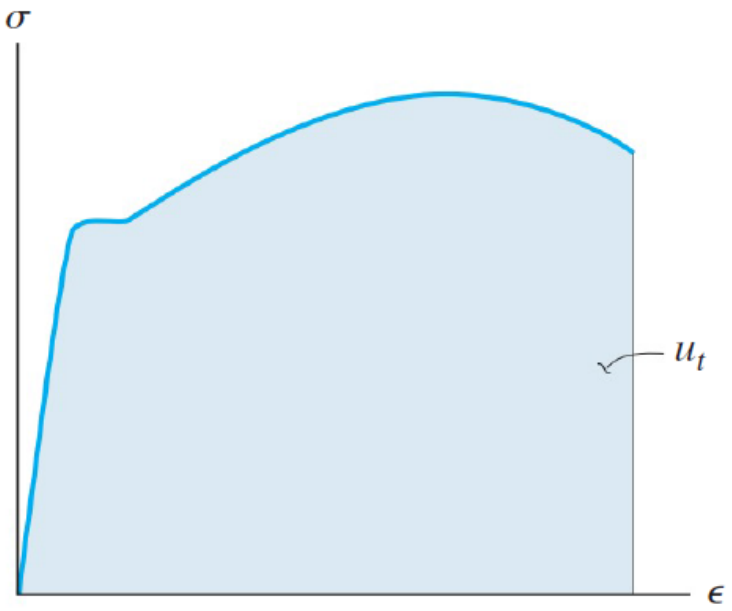

Figure 2.3: Modulus of Toughness from Stress-Strain Graph [6]

2.1.4 Deformation at High Strain Rate

The rate of deformation of a material when exposed to external stresses is known as strain rate. High temperature deformation processes which are dependent on time vary much significantly than low temperature deformation processes. Deformation process at room temperature becomes fully adiabatic when strain rate is increased. When strain rate becomes much higher, this rise in temperature because of adiabatic heat doesn't have much time to discharge out of the material through deformation procedure. This result in adiabatic shear uncertainty that incorporates a deep effect on mechanical behavior of material. Adiabatic shear bands (ASB) are produced as a result of thermal softening induced because of taking place of adiabatic heating in a very small area [10]. Adiabatic shear bands are very thin areas with extremely deformed material due to high strain rate forces. They not only lead towards additional damage but sometimes leads to complete fracture in some situations. Loading in material at high strain rate results in shock

waves which in turn create adiabatic shear bands. Region covering adiabatic shear bands are usually brittle than overall material and are reason of failure in numerous cases below dynamic loading.

- **Adiabatic Shear Bands:** The rise in internal temperature as result of plastic deformation and friction at impact area in strain rate dependent and high velocity impact problems, doesn't have enough time to spread out from the area. Hence, such section starts behaving adiabatically which in turns results in enormous heat generation, huge plastic deformation, thermal softening and sometimes fracture. This process is called adiabatic shear localization which creates adiabatic shear bands. Velocity of the impact decides localization of adiabatic shear bands. Meshless numerical strategies are being used to study adiabatic shear bands in many recent studies. It is a fact that technology existing nowadays is believably not able to capture formation of adiabatic shear bands because it requires much smaller size mesh which may produce distortion in elements during analysis.

2.2 Impact Loading Failure Mechanism

A comprehensive research study of mechanics of impact and penetration is required to comprehend material's response to impact loading. Hence, a thorough background and literature review is vital to succeed in this research. Successful analysis of ballistic response of high hardness perforated armor steel plates when impacted with armor piercing projectiles.

Isotropic materials such as metals have uniform properties in each direction. Perforation of metals caused by impact forces are driven by conversation laws. Kinetic energy of the projectile transmits into the armor steel plate upon impact of plate with incoming projectile. This causes deformation in the armor plate due to increased internal energy. Kinetic energy of projectile also gets dispersed in form of heat and light in the environment and also in fragments of armor plate broken due to impact. These types of energy are much problematic to determine.

Impact loading can be defined as a high shock or force applied over a short-lived period of time. The relative velocity among projectile and the armor steel plate outlines the severity of impact. During impact, projectile's kinetic energy is absorbed into the armor steel plate. Same kinetic energy is converted to strain energy of the armor steel plate. Impacted area of the armor steel plate will be deformed and deformation in material will be depending upon the kinetic energy

of the projectile. Consequently, greater deformation will happen in material when it is impacted with higher velocity projectile as it will induce more deformation energy. Nevertheless, if deformation energy in the armor steel plate surpasses endurance of that plate, projectile will pierce through the target plate [11]. Different fracture mechanisms of armor plates are displayed in figure 2.4.

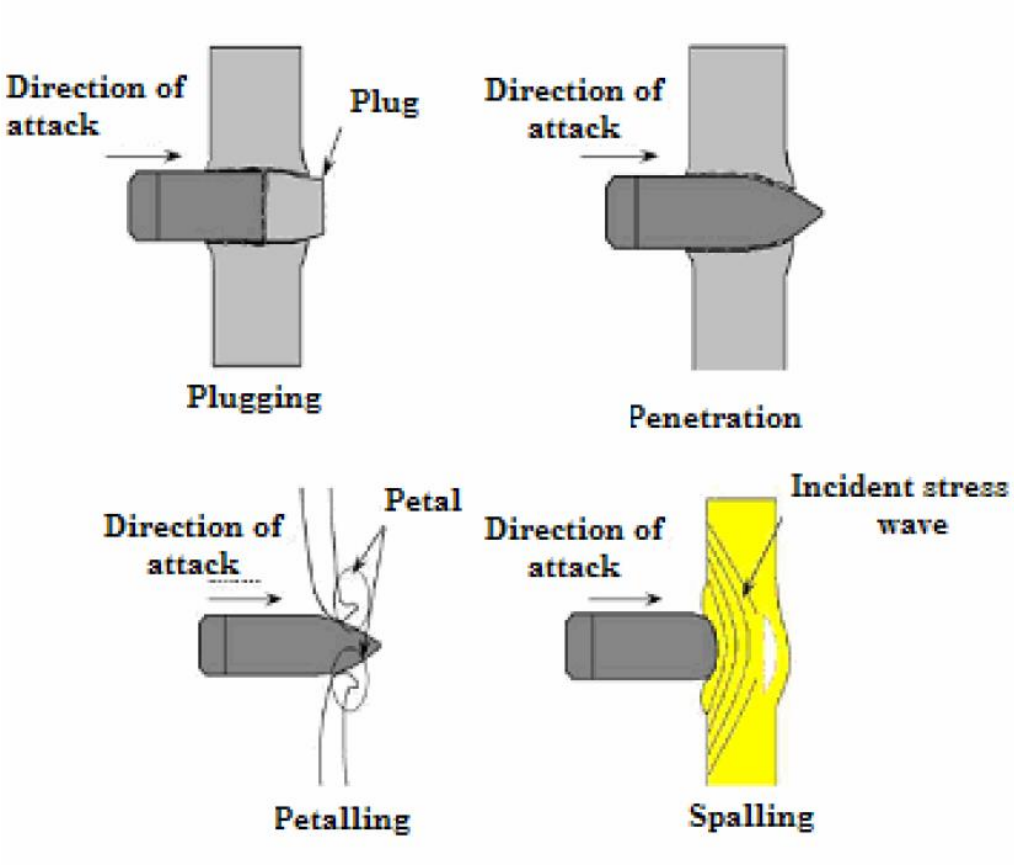

Figure 2.4: Fracture Mechanism in Armor Plates [12, 13]

- **Plugging Fracture:** When a blunted or hemispherical shaped projectile hits armor plate with a much higher velocity closer to the materials ballistic limit, fracture mechanism of plugging happens. Thus, creating impact of identical size on the armor plate [13].
- **Petalling Fracture:** Due to extreme circumferential and radial stresses, armor plate fractures from initial stress waves which is known as petalling fracture. Tip of the projectile has the maximum stress. The distinguishing failure shape is caused by bending stresses produced due to inward motion of projectile inside of the armor plate.

This can be seen when a thin plate is impacted by a conical projectile at velocity comparatively lower than the ballistic limit [13, 14].

- **Penetration:** The fracture that happens when a bullet perforates inside the armor plate beyond spall crater's thickness is known as penetration. Measure of crater depth cross section is called penetration depth [12, 13].
- **Spalling Fracture:** The fracture mechanism when the armor plates fracture as outcome of echoed impulse from distal face of armor plate due to projectile's impact, is called spalling. It happens in material that have more compressive strength then tensile [12, 13].

2.3 Materials Used in Armoring

There a many criterion which can be used when selecting material for an armor system while remaining in allowable price and volume. None of material could be selected as best material for armoring. Because a material providing protection against a threat can be inadequate for threat in any other threat scenario, particularly if either or volume or both are required to be lessened [15]. Following materials are commonly used in armoring:

- **Wrought Iron:** Wrought iron is used for cladding war ships [16].
- **Rolled Homogenous Armor:** Rolled Homogenous Armor is made up to hardened steel and a high velocity projectile can't shatter this material [17].
- **Ceramics:** Ceramics are commonly used in armoring especially as composite with different materials. Silicon Carbide, Silicon Nitride, Boron Carbide, Aluminum Oxide and Tungsten Carbide are normally used in armoring application [18].
- **Glass:** Glass commonly labeled as Bullet Proof Glass is also used for transparent armor in vehicles and other structures built for surveillance [18].
- **Aluminum:** Aluminum metal is usually used in light weight armored vehicles [19].
- **Depleted Uranium:** Depleted Uranium of high density is sandwiched between armor plates in tanks for higher protection [20].
- **Plastic:** Plastic can deflect incoming projectile's trajectory and are enormously effective against armor piercing projectiles [21].
- **Titanium:** Titanium is also considered as one of the potent armoring material but due its much high cost it is not economical to use [22].

- **Composite Materials:** Composite materials are widely used in arouring and reinforcing applications [23]. Three main classes of composite materials are depicted in figure 2.5 which are structural composites, fiber reinforced composites and particle reinforced composites.

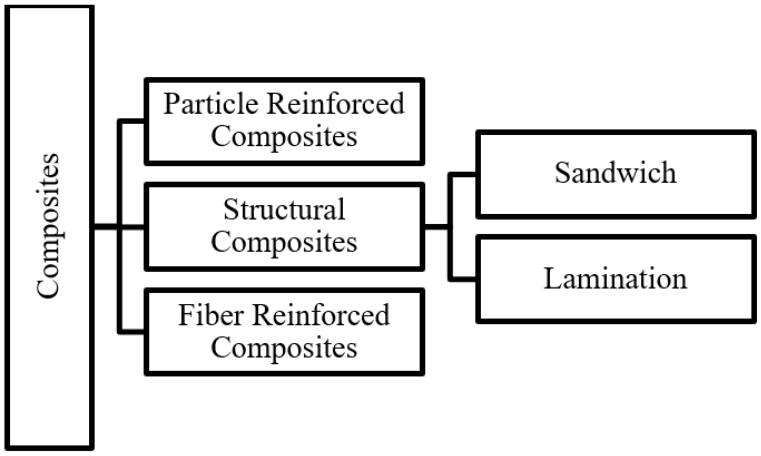

Figure 2.5: Classes of Composites

2.4 Ballistic Impact Numerical Analysis Models

During last three to four decades, many scholars have been trying to interpret behavior of high velocity impact by studying the high strain rate response of different materials. Research scholars have been deploying new methods and programs with advancement of technology. The newly developed numerical analysis methods are providing a more accurate and closer to reality picture of impact response to the researchers. Numerical analysis methods also save enormous experimental cost which would have incurred. This research also presents similar study concerning ballistic response of high hardness perforated armor steel plates.

Designing lighter weight armor is a complex job and hence, requires a thorough grasp on every phase of impact progression. For development of lighter weight armors, numerous alternative models are available. Foremost and most accurate method is experimentation, but experimentation is not economical viable due to heavy finance and skilled personnel requirement for carrying out high velocity impact very accurately. After experimentation, software based numerical models provide a comprehensive apprehension of impact and fracture mechanism along with support in developing enhanced armor design. The software based numerical models can

simulate much intricate analysis of different projectile in turn reducing cost and time to be incurred in experimentation [24].

Modelling of impact loading mechanism along with demonstration of fracture criteria and project proliferation has been conducted in different comprehensive studies. Projectile proliferation and cracking of Weldox 460 E material, which rolled steel with high strength, was demonstrated by Børvik et al. using explicit finite element analysis in LS-DYNA software [25]. It was found that mesh sensitivity is very vital in finite element analysis model. Nazeer et al. successfully illustrated mathematical model for piercing and failure progression target of ductile metals [26]. Following inferences were made by Nazeer et al. after research:

a. A numerical analysis method was devised to evaluate failure toughness of a ductile material.
b. With decrease in cone angle of tool, target bending angle also decreases nearly linearly.
c. Same results can be replicated on NS4 Aluminum and SIC half hard sheet.
d. Using Rigid Plastic Failure Mechanics, toughness of sheet of ductile metals can be determined mathematically.
e. The process can be used to determine failure toughness and quantity of petals to be formed.
f. It was found that optimum behavior of parameter is characteristic of tools with conical tip and this cannot be seen in tools with sharp and ball shaped tip.

Liu et al. investigated impact of a cylindrical projectile on target and determined critical thickness of target plate and relative deformation occurred in target and projectile after impact [27]. They illustrated deformation and changes in projectile shape from impact to the failure along with projectile deformation after piercing through metal plates.

Rusinek et al. predicted damage progression in sheets of mild steel upon hemispherical projectile's impact through numerical model and experimentation [28]. Their study illustrated formation of petal in sheet of metal and demonstrated damage progression in target plate. Their research found finite element analysis technique results regarding petal dislocation much closer to the results obtained through experimentation. Many researchers have comprehensively studied and precisely forecasted performance of different classes of composites including fiber reinforced composites, fabrics and soft laminates [29-41].

Ratio of thickness of ceramic and metal plate in composite armor system against 47 grams steel projectile and7.62 mm armor piercing hard core bullet was optimized by Lee and Yoo [33]. Least ratio came out to be 1.5 and 3 respectively. Both experimental and finite element analysis technique were used by these researchers. Result of finite element analysis through simulation were identical to results of experimentation. Hence, finite element analysis method can be used for design and development of ceramic and metal composite armor systems.

Wang et al. studied perpendicular impact of projectiles having cone shaped tip on aluminum oxide tiles backed by aluminum target plates [32]. It was observed that conical rupture pattern occurs in tip of projectile. An empirical method was developed for minimum kinetic energy needed to penetrate a metal plate. Base plate optimum thickness was found out to be a function of material fracture mechanism and damage progression. It was also noted that failure progression speed in aluminum oxide is approximately 3000 m/s which much lower than speed of shock wave in aluminum oxide roughly 10,000 m/s [42] which support in delaying weakening of impact resistance of material.

Espinosa et al. investigated response of ceramic layered steel targets against high velocity impact through finite element analysis [34]. Depth of penetration was found to be extremely dependent on configuration of ceramic steel armor system. Depth of penetration was found to be independent to ceramic material structure.

High hardness perforated steel plates in different configurations and design are being used in defence industry. The holes and perforations configured in a systematic pattern, are specifically developed for high hardness perforated steel plates [43]. In 1986, Ben-Moshe developed high hardness perforated steel armor for armored personnel carriers [1]. The design of holes must be in such a way that its diameter must be lesser than the diameter of caliber, it is designed to defeat. Triangle shaped perforations on high hardness armor steel plate were developed by Auyer et al in 1991 [2]. Ravid and Hirschberg introduced an armor system for defeating small calibers having a secondary perforated plate with 40~50% area covered with perforations [3]. Smith and Norris improved design of slot shaped perforations thus reducing weight up to 50% than solid plate [4]. US Army has used such high hardness perforated steel plates in armored personnel carriers to counter threat of small caliber ammunition and are known as P900. The addition of high hardness perforated steel plates on armored personnel carriers as add-on armor improved their mass efficiency [44].

Use of geometric perforation to increase protection was found in some patents [1-3, 19] but studies pertaining to experimentation and finite element analysis in this area are much less. Balos et al. illustrated ballistic response of impact of 12.7 mm projectiles on perforated plates by investigating effect of thickness, geometry, inclination of plate, distance between perforated plate and base plate and mechanical properties [45]. Radisavljevic et al. made an effort to design effective high hardness perforated steel armor by optimizing diameters and distances of perforations [46]. Mishra et al. found experimentally that impact resistance of armor target plate can be enhanced intensely by designing a symmetrical perforation pattern on it [47, 48]. Feasibility of usage of various grades of steel in development of high hardness perforated armors was done by Howell et al. [49]. Chocron et al. investigated numerically the impact and fracture mechanism when 7.62 mm armor piercing projectile impacts on edge of target armor plate [50] and calculated strain and bending developed because of projectile. Rosenberg et al. illustrated through finite element analysis and experimentation the fragmentation of armor piercing projectile when impacted with high hardness steel plate mounted at inclination [51, 52].

High velocity impact includes strain rate dependent shattering, erosion and deformation in material in ballistic scenarios. Hence, to get precise response, a numerical simulation model needs to take aforementioned factors in to account. New softwares and methods provide much realistic image of response of plate upon impact. Most of researches use continuum hydrodynamic codes to explore ballistic response as illustrated by thorough literature review on numerical analysis simulations of high velocity impact ballistic problems [53-55]. LS-DYNA, ANSYS AUTODYN and Abaqus CAE are frequently used in explicit dynamics analysis to simulate response of armor materials against different types of threats.

Ballistic response of Weldox 460 E steel upon impact of high velocity cylindrical projectiles was investigated by Børvik et al. using Johnson-Cook plastic and damage model [56]. Due to unavailability of projectile's material data, projectile was modelled using linear elastic material model with Poisson's Ratio of 0.33 and Modulus of Elasticity of 200 GPa. Performance of steel armor upon impact of 7.62 mm armor piercing projectile using spall failure model for hardened steel projectile was done by Buchar et al. [57] and found results of experimentation and simulation much closer. Effect of shape of projectile on ballistic response was determined by Børvik et al. using LS-DYNA [58]. Ballistic response of double layered steel and resistance of Weldox 700 steel and monolithic steel against high speed projectiles were determined by Dey et

al. [59] and Teng et al. [60] respectively using Johnson-Cook plastic and damage model. Børvik et al. did a thorough study on ballistic response of various types of hardened alloys of steel against high velocity projectiles and compared numerical model with experimentation [61].

CHAPTER 3: EXPERIMENTATION

3.1 Ballistic Experimentation

An important part is played by ballistic experimentation to understand primary and perilous major issues pertaining to mechanics of armor, its composition and its applications. An authorized and reliable data of experimentation is needed to validate results forecasted by finite element analysis. Excessive safety procedures are required to conduct experimentation of high velocity projectile's impact on target. A brief description of noteworthy experimentation has been given below. These ballistic experimentations and tests are usually performed in defence departments authorized by the government for guaranteeing the safety of observer, researcher and other individuals. Hence, standards and codes of ballistic testing must be implemented for precise results and safety.

To depict performance of a ballistic material, V_0 and V_{50} are the two typically applied experimental procedures. The velocity at which ballistic projectiles of known shape and mass are stopped and defeated by the target is known as V_0 while the velocity at which 50% or half of the fired rounds of projectile having known mass and geometry pass through the target is called V_{50}. Material's ballistic limit is the velocity at which a certain projection when fired at a specific angle, penetrates the material. Ballistic limit technique is also used in experimentation. Another method generally used to assess protection provided by material in reenactments is decreasing kinetic energy of projectile upon impact with the target.

During research on ballistic performance, it is rudimentary to determine performance of protection by backing with dense deposit of clay for finding the depth of projectile by measuring impression made in clay. In testing of bullet proof helmet same method is used, however clay is filled into a head like casting and fitted into the helmet. An armor plate of predefined thickness in mounted on a stand in desired spot and distance from position of gun or launcher in typical ballistic experimentation. For acquiring required data from experimentation, specialized instruments and equipment are used. Very handy linkage between experimentation and numerical analysis is provided by penetration depth of projectile. Diameter of perforations is also critical parameter in determining the fracture of armor material.

Preece et al. provided hydrocodes data and experimentation data of steel, Kevlar and Kevlar-Steel composite against copper-lead projectiles [62]. Orphal et al. used x-rays to visualize

target-projectile interaction at the time of impact [63] and using this data, parameters including penetrator's remaining length as function of time, depth of penetration as function of time, final depth of penetration and velocity of projectile while penetrating the target were measured.

Many scholars have used high speed imaging techniques to study ballistic interactions during last few years which help in capturing critical moments of ballistic proliferation. Digital high speed camera was used by Børvik et al. to visualize projectile's infiltration process [56]. The image converter camera delivers very fast shutter speeds, whereas the Charged Coupled Device camera provides digital images instantly after the experimentation. The data collected was used to find velocity. A photocell system with two similar LED on top and detector on bottom of path of projectile were installed to measure initial velocity of projectile. A similar system with six lasers mounted on each LED was installed to measure residual velocity of projectile [56]. Various estimation methods being deployed by researchers are as under:

1. Capability of penetration of a projectile and hole sweep [62]
2. X-rays for visualizing target-projectile interaction during impact [63, 64]
3. Photocell systems to measure velocity [65]
4. High Speed Imaging to witness penetration process during impact [56, 66]

In ballistic experimentation, following two scenarios can occur either projectile hits the armor and disintegrates into various fragments or the projectile penetrates the armor material. The four phases of bullet velocity that have been described by different researchers are as under:

1. Free flight of projectile
2. Interaction with target on impact
3. Perforation into the target
4. Subsequent flight after penetration

3.2 Material Characterization

Material under low strain rate deformation can be characterized through standard mechanical testing procedure using servo hydraulic equipment [67]. But ballistic responses are extremely dynamic in nature and are driven by strain rate. The loading depending on strain rate can be classified into three types: low strain rate loading ($\varepsilon < 0.1\ s^{-1}$); medium strain rate loading ($0.1\ s^{-1} < \varepsilon < 100\ s^{-1}$); and high strain rate loading ($\varepsilon > 100\ s^{-1}$). Tests are required to define material

properly through complete range of strain rate. Following are various methods used for estimating medium strain rate loading and high strain rate loading:

3.2.1 Medium Strain Rate Loading Estimation

Loading having strain rate between 0.1 and 100 per second are at medium strain rate and require forced procedures for measuring strain rate. Load assessment will have some influence from creation of shock wave. Automotive sector uses such systems for illustrating safety of their automobile during crash. Drop Tower is one of such instruments, in which load falls on material under investigation from a height freely under influence of gravity (can be assisted by hydraulics if high speed is required). Figure 3.1 depicts one of such instruments.

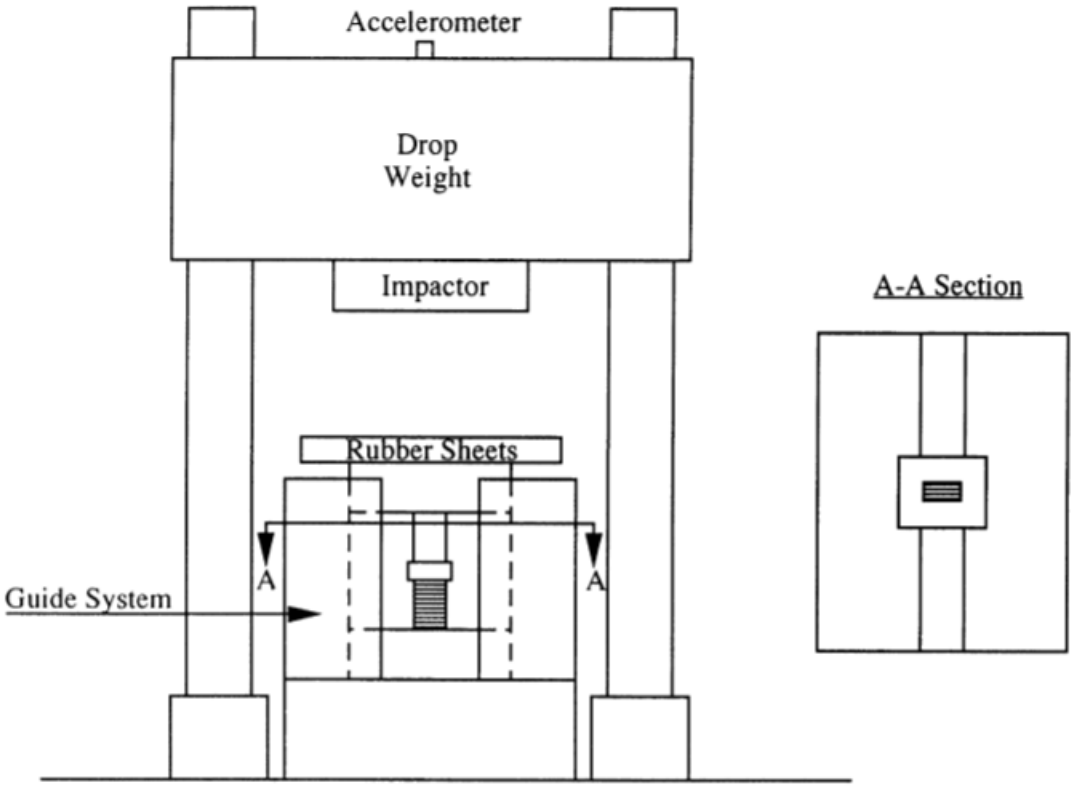

Figure 3.1: Drop Tower Apparatus [67]

Stress-Strain response is calculated by employing data from accelerometer and velocity of impact. This impact experiment is much realistic and can be used on various geometries and allows to vary strain rate easily. The drawback is that creation of shock wave is not taken in account. For more precision, standard mechanical testing procedures are incorporated with hydraulic servo motor with a limiting controller. More precise stress-strain relation can be obtained through this

assembly. It also has disadvantage of not taking creation of shock wave into account and huge financial impact.

3.2.2 High Strain Rate Loading Estimation

Normal strain rate estimation apparatus can't be used at high strain rates due to greater distortion properties and minute loading time of impact. Bertram Hopkinson developed a system for linking connection between pressure and time to forecast projectile's effect on target [68]. A compressive pressure wave was produced by hitting one side of rod. At other side of rod, a steel bar is attached with help of lubricating grease. Upon hitting the end of rod, compressive pressure wave is generated which travels through the rod. As rod lubricating grease is not capable of holding steel bar on the end of rod, the compressive wave will cause the steel bar to fly off with certain velocity which will be measured by ballistic pendulum [69].

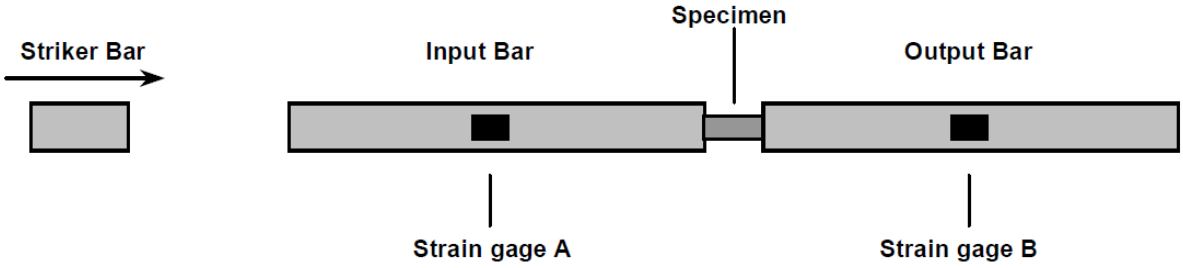

Figure 3.2: Split Hopkinson Pressure Bar's Schematic [69]

Kolsky added a secondary pressure for enhancing Hopkinson apparatus and built Split Hopkinson Pressure Bar apparatus [70]. For exploring material's response to high strain, Split Hopkinson Pressure Bar is mostly used [71-73]. Figure 3.2 depicts setup of Split Hopkinson Pressure Bar.

3.3 Experimental Setup

Experiments of ballistic testing were performed to determine the response of standalone base armor plate and its combination with these three types of high hardness perforated plates. The base armor plate was of aluminum of grade AA5083-H116. The aluminum AA5083-H116 is magnesium alloy of aluminum with magnesium greater than 3% wt. This alloy is one of highest strength alloy of aluminum. Its best suited for making rolled plates and is used for protection purposes and marine applications. The aluminum base armor plate was 38.1 mm thick (Figure 3.3).

Figure 3.3: Aluminum AA5083-H116 Base Plate side view

The high hardness perforated plates were manufactured from Ballistic Steel SECURE 500, which is a standard grade for protection against hard core projectiles. SECURE 500 has good workability, weld ability, cold forming and high hardness value. The dimensions of high hardness perforated plates were 304mm x 307mm x 8mm. The three case of perforations were made.

- Circular Perforations
- Diamond Shaped Perforations
- Slot Shaped Perforations

The high hardness perforated plate was separated from base armor plate using spacer of 110mm and was securely bolted (Figure 3.4 & 3.5).

Figure 3.4: High Hardness perforated plated mounted on Aluminum Base Plate

Figure 3.5: High Hardness perforated plated mounted on Aluminum Base Plate Side View

The multi layered armor plates were impacted by 7.62 x 51mm AP hard core bullet. The bullet has an outer Brass jacket and inner steel core [74] (Figure 3.6).

Figure 3.6: 7.62 mm Armor Piercing Bullet

The velocity of projectile was measured using a chronograph, which was placed 1 m away from the rifle in direction of target. Three bullets were fired on each of the multi layered steel armor plates to determine ballistic response. The projectile velocity was found between 860~920 m/s. All experiments were recorded using a High-Speed Camera manufactured by Vision Research, United States.

3.3.1 Case 1: Monolithic Base Plate

In case 1, ballistic response of 38.1 mm thick monolithic base plate was observed. Experimental setup is depicted in figure 3.7 shown below. It consisted of base aluminum plate, high speed camera, gun and chronograph. The chronograph was placed 1 meter from the gun. Base aluminum armor plate was placed 10 meters from the gun as shown below.

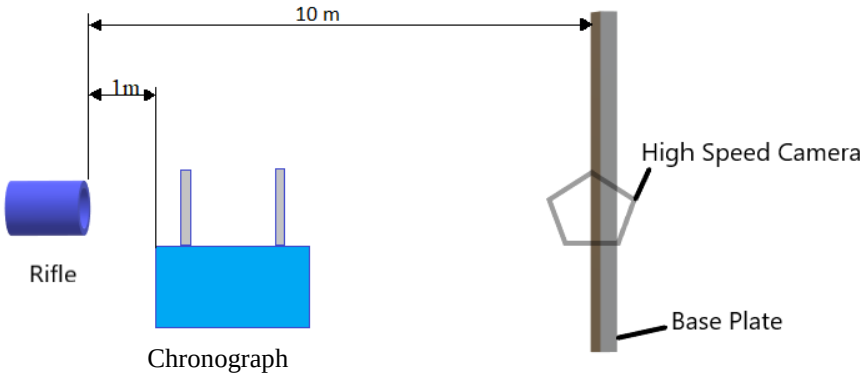

Figure 3.7: Experimental Setup for Base Aluminum Plate (not to scale)

3.3.2 Case 2: Base Plate with High Hardness Steel Plate with Circular Perforations

In case 2, ballistic response of 38.1 mm thick monolithic base plate fitted with high hardness steel plate with circular perforations was observed. Experimental setup is depicted in figure 3.8 shown below. It consisted of base aluminum plate, high hardness steel plate with circular perforations, high speed camera, gun and chronograph. High hardness steel plate with circular perforations is fitted 0.110 meters in front of aluminum base plate. High hardness perforated plate is 8 mm thick.

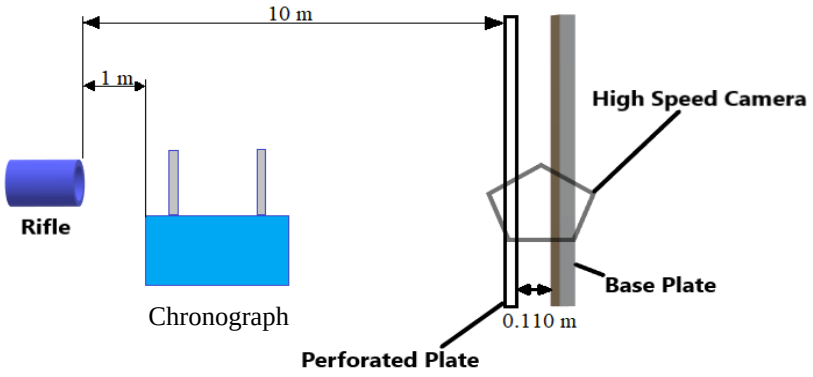

Figure 3.8: Experimental Setup for Base Aluminum Plate with Perforated Plate (not to scale)

3.3.3 Case 3: Base Plate with High Hardness Steel Plate with Diamond Shaped Perforations

Case 3 has setup similar to case 2 with diamond shaped perforated plate instead of circular perforations.

3.3.4 Case 4: Base Plate with High Hardness Steel Plate with Slot Shaped Perforations

Case 4 also has setup similar to case 2 and 3 with slot shaped perforated plate instead of diamond shaped or circular perforations.

Results of experimentation will be discussed in later chapter along with results of numerical simulations. It was found that the steel core of 7.62 mm armor piercing round is much hard than other components of the bullet and is key reason behind fracture of aluminum base armor plate. Hence, only steel core will be considered during numerical simulations.

CHAPTER 4: FINITE ELEMENT ANALYSIS CODES

Finite element analysis technique is most precise numerical analysis method to explore the basis of many complex mechanical and structural problems. Amid various critical and valued tools available to scholars, it has developed its importance. The quality of numerical analysis and simulation depends upon definition of basic parameters of the problems. Various finite element analysis codes together with high speed computational devices, are available now that can be used to get solutions of many mechanical problems. Simulia Abaqus, LS-DYNA, MSC NASTRAN, MSC DYTRAN, Ansys, COSMOS and many other finite element processors are available nowadays. To augment these processors, various pre-processors have also been developed. Abaqus CAE will be used in our research for numerical simulations.

4.1 Abaqus Software

Dr. David Hibbitt, Dr. Bengt Karlsson, and Dr. Paul Sorensen developed Abaqus in 1978. Abaqus was developed to help researchers to create their customized material models. It has now capability to solve various mechanical problems including linear/standard and non-linear/explicit problems through finite element analysis models. Abaqus CAE (Complete Abaqus Environment) possess graphical environment for visualizing the problem. Abaqus can create and import parts for meshing. Abaqus CAE has capability of creating assemblies, assigning material models, applying forces, defining boundary conditions and presenting result after processing. It has two key modules for analysis; Standard and Explicit.

4.1.1 Abaqus CAE Standard Module

Standard module of Abaqus CAE is commonly used in problems ranging from linear to non-linear regimes including; temperature, electrical, static and dynamic responses of materials. At each increment, Abaqus CAE Standard Module solves mathematical equations' system implicitly.

4.1.2 Abaqus CAE Explicit Module

For explicit dynamic analysis using finite element analysis techniques, explicit module of Abaqus CAE is very promising simulation software. Instead of solving mathematical equations at

each increment, like in standard module, it creates a time-based solution at each minute step of time. Abaqus CAE Explicit module is used in studying transient and explicit problems involving impact and explosion conditions.

4.2 Formulation Principles

Lagrange, Euler and Smooth Particle Hydrodynamic formulation will be discussed in this section.

4.2.1 Lagrange Method

One of the most extensively used numerical analysis technique is Lagrange formulation especially for experimental purposes. As per Lagrange formulation each object has exclusive nodal points. This means that every nodal point has a unique direction. Elements are made by combining various nodal points. Nodal points are forced to translate and change in body's shape occur upon deformation. In langrage method pertaining to perforations, wide distortion in elements is one of vital concern. For good quality mesh, convergence study is significant. For allowing simulation to progress, highly damaged elements can be deleted using material removal parameter. These removed elements are illustrated with high accuracy.

4.2.2 Euler's Equation

Euler's equation is usually used for studying fluid and other flowing materials. A Eulerian equation can be applied when a projectile or armor materials undergo high distortions causing softening in material. Material is deliberated as "Stagnant Frame of Reference" in which elements along with their mass and force moves from one nodal point to other. Mesh generated through Eulerian method should be large to apprehend all particular details of flow of material upon disfigurement.

4.2.3 Smooth Particle Hydrodynamics Formulation

Smooth Particle Hydrodynamics is mesh free system that are connected for unbalanced scenarios having high deformations. Smooth Particle Hydrodynamics fills gap of Euler and Lagrange methods [75]. Free nodal points with different mass are called elements which have understanding for function interpolation.

4.3 Models for Dynamic Fracture

The models for dynamic fracture are default methods for illustrating and examining the damage and fracture of object in Abaqus software. Both static and dynamic loading problems can be studied through these models. Abaqus Explicit has two criteria i.e., Shear Failure Model and Ductile Failure Model, for depicting materials under high strain rate. Plastic yield of material is used as key fracture starting point in shear failure method. Whereas, elastic limits are viewed as key fracture starting point in ductile failure method. These models can be applied to limit forces on elements (till element removal point) when maximum stress value is touched. For same material both criteria can be employed at same instance.

4.3.1 Shear Failure Model

Material shear failure model hinges on approximation of plastic deformation proportion at nodes of elements i.e., when rate of critical damage value goes to unity, damaged elements wear out. The damage variable "ω" is given by following formula,

$$\omega = \frac{\varepsilon_o^{pl} + \sum \Delta\varepsilon^{pl}}{\varepsilon_f^{pl}} \tag{7}$$

Where ε_o^{pl} is plastic strain initial value, $\Delta\varepsilon^{pl}$ is known as strain increment equivalent and ε_f^{pl} is strain at fracture and total damage parameter can be found by addition of total increase in analysis. The fracture strain ε_f^{pl} hinges upon value of plastic strain rate ε_o^{pl}, ratio of stress (p/q, where p is pressure stress and q is Von Mises Stress), temperature and other field parameter. The shear fracture model is projected fir high strain rate problems pertaining to various material, usually metals. It utilizes the proportionate plastic strain for fracture instigation. It can be used with both Von Mises criteria and Johnson Cook plastic criteria. The shear fracture model can be applied as a piece of tensile fracture model.

4.3.2 Tensile Failure Model

Hydrostatic pressure limit is used to analyze dynamic spall for element damage in tensile fracture model of Abaqus Explicit. When pressure limit rises more than hydrostatic stress limit of material, tensile fracture happens. Hydrostatic stress limit hinges upon temperature of body and other field parameters. There is no default value of hydrostatic stress limit. Tensile fracture model

is occasionally used with equation of state models in addition to its usage with Von Mises criteria and Johnson Cook plastic criteria. Tensile fracture model is used for high strain rate failure of many metals and other materials. It uses hydrostatic mass as scale to model spall of element. It provides different scenarios of failure including removal of elements. It can also be used as piece of shear fracture model.

4.4 Fracture Decision

At point of initiation of tensile or elastic failure at node, elements of material start failing. Five models i.e., element removal due to element erosion during fracture and four spall models due to shock wave generation by distal side of target, are presented in tensile fracture criterion.

4.4.1 Element Removal

All stresses become nil and material failure happens, when tensile fracture occurs at an integration point. Whenever tensile fracture parameter reaches to unity, element removal occurs by default. Fracture or erosion of every element is not required for total fracture of material. At failure of nodal points, element destruction occurs in first order solid elements. In order to remove element from mesh, all nodal point in direction of thickness must erode in shell elements. Fracture happens in second order beam elements when nodal points fail at two element integration in direction of axis of beam. Failure of any nodal points causes removal of tetrahedral and triangular elements.

4.4.2 Spall Models

In lieu of element removal, spall model is an alternative fracture model which has four fracture groupings available. On occurrence of tensile fracture, deviatoric stress may or may not be equal zero at integration point. Also, limiting pressure may or may not be limited by hydrostatic stress limit. Hence, four fracture permutations are as under:

1. **Ductile Shear and Brittle Pressure** – Stress component is not affected. Compressive stress will give pressure stress.

2. **Brittle Shear and Brittle Pressure** – Stress component equals to zero and will continue to be zero during remaining analysis. Compressive stress will give pressure stress.
3. **Ductile Shear and Ductile Pressure** – Stress component is not affected. Hydrostatic stress will give pressure stress.
4. **Brittle Shear and Ductile Pressure** – Stress component equals to zero and will continue to be zero during remaining analysis. Hydrostatic stress will give pressure stress.

CHAPTER 5: FINITE ELEMENT ANALYSIS MODELLING

In a numerical model, material is studied by distributing then into distinct minute elements. Various numerical analysis techniques are available to make these distinct elements in material. Euler, Lagrange, Arbitrary Langrage Euler (ALE) are most commonly used techniques for creating elements. Meshless techniques, like Smooth Particles Hydrodynamics (SPH) are also used. For illustrating deformations in target material, Lagrange technique is more accurate than Smooth Particles Hydrodynamics. Material movement and particular details in low deformed area are illustrated accurately because mesh moves with material in Lagrange formulation. This preciseness is comprehensively utilized because of its ability to capture material interface effectively. In highly deformed zone, numerical matrix becomes much distorted and jumbled which in turn causes negative influence on step time and accuracy in Lagrange formulation. Wide elemental distortion causes zero or negative element volume in few cases. This can be solved by deploying substitute and effective meshing strategies. This will require increased computational power but will enhance results. Following material models are used in numerical analysis methods:

5.1 Johnson Cook Plasticity Model

In high strain rate dependent problems, Johnson Cook Plasticity Model is mostly utilized for modelling [76]. It is present in commercially available finite element analysis packages and is usually used to simulate ballistic and impact scenarios numerically. The elastic rate dependent behavior of ductile materials is described by this model. Effect of strain, strain rate hardening and thermal softening on flow or material's yield stress is also depicted by Johnson Cook Plasticity Model. Johnson Cook Ductility Model can be written as [76-78]:

$$\sigma_y = [A + B\varepsilon^n][1 + C \ln \dot{\varepsilon}][1 - T^{*m}] \quad (8)$$

Where "ε" denotes strain, "n" is strain hardening exponent,"$\dot{\varepsilon}$" denotes plastic strain rate which is ratio of equivalent plastic strain rate to reference strain rate and is expressed is equation 9, "A" is yield stress at reference strain rate and reference temperature, "B" is coefficient of strain hardening, "C" is strain rate hardening coefficient and "m" is thermal softening exponent. Where T^* is homologous temperature which is given by equation 10 [77].

$$\dot{\varepsilon} = \frac{\text{equivalent plastic strain rate}}{\text{reference strain rate}} = \frac{\dot{\varepsilon}}{\dot{\varepsilon_r}} \quad (9)$$

$$T^* = \frac{\mathrm{T} - T_r}{T_m - T_r} \tag{10}$$

Where T_r is reference temperature and T_m is melting temperature in kelvin scale.

5.2 Johnson Cook Damage Model

With addition of tri-axis stress, strain rate and temperature on material, Johnson Cook Damage model is extended failure strain model. A material fractures when damage parameter reaches a critical value as per Johnson Cook Damage model. The damage parameter can be expressed as:

$$\mathrm{D} = \sum \frac{\varepsilon_p}{\varepsilon^f} \tag{11}$$

At "D" equals to zero, material is undeformed while when "D" approaches unity, material fails. According to this model, the strain energy can be found empirically as:

$$\varepsilon^f = (D_1 + D_2 \exp(D_3 \frac{\sigma_m}{\sigma_{eq}}))(1 + D_4 \ln \dot{\varepsilon}_p^*)(1 + D_5 T^*) \tag{12}$$

Where D_1 to D_5 represent damage constants, σ_{eq} is equivalent stress and σ_m is mean stress [78, 79].

5.3 Mie-Grüneisen EOS

In this research, Mie-Grüneisen Equation of State (EOS) is employed for simulation. Modelling of materials under high pressure is done by Mie-Grüneisen Equation of State (EOS). Table 5-1 provides values of Mie-Grüneisen Equation of State (EOS) parameters for aluminum base plate, high hardness perforated steel plates and core of 7.62 mm armor piercing bullet.

5.4 Properties of Materials Used

Abaqus CAE is used to simulate conducted experiments through finite element analysis techniques. Kılıç et al. used Lagrange formulation for meshing in numerical analysis [74], same is used in this research. Much precise results are obtained using Lagrange formulation as compared to Smooth Particles Hydrodynamics Method which is meshless. High distortion in mesh is the only concern in using Lagrange formulation because it can produce error in results of simulation. Hence, mesh size is vital to numerical simulation in this research. Four cases of ballistic impact were simulated as in experiments:

1. Case 1: Monolithic Base Plate
2. Case 2: Base Plate with High Hardness Steel Plate with Circular Perforations
3. Case 3: Base Plate with High Hardness Steel Plate with Diamond Shaped Perforations
4. Case 4: Base Plate with High Hardness Steel Plate with Slot Shaped Perforations

In case 1, the numerical model includes aluminum AA5083-H116 base plate of thickness 38.1 mm and 7.62 mm armor piercing bullet's core. Dimension of bullet core were taken from Kılıç et al. [74]. Table 5-2 provides values for material parameters along with parameters of Johnson Cook Fracture model for aluminum base plate and damage parameters for core of bullet. In case 2, 3 and 4, aluminum base plate has been covered with high hardness perforated steel plates at distance of 110 mm. Parameters related to Mie-Grunisen EOS and Johnson Cook Failure model for high hardness steel plate were used from Kılıç et al. [5].

Table 5-1: Material Parameters

Parameter	**Symbol**	**Unit**	**AA5083-H116 [80]**	**Bullet Core [74]**	**Steel Secure 500 [74]**
Melting Temperature	T_m	K	893	1800	1800
Density	ρ	kg/m^3	2700	7850	7850
Poisson's ratio	v	-	0.3	0.3	0.3
Elastic Modulus	E	GPa	-	206	206
Specific heat at constant pressure	C_p	J/kg.K	910	477	450
Shear Modulus	G	GPa	70	80	80

Table 5-2: Johnson-Cook Parameters

Parameter	**Symbol**	**Unit**	**AA5083-H116 [80]**	**Bullet Core [74]**	**Steel Secure 500 [74]**
Initial yield stress	A	MPa	167	1900	1200
Strain hardening Coefficient	B	MPa	596	1100	1580
Strain rate	C	-	0.001	0.05	0.004

Coefficient					
Strain hardening Exponent	n	-	0.551	0.3	0.175
Thermal softening Exponent	m	-	0.859	1	1
Reference strain Rate	$\dot{\varepsilon}_o$	1/s	1	1×10^{-3}	1×10^{-4}
Room Temperature	T_r	K	293	300	300
Johnson-Cook Failure	D_1	-	0.0261	Undefined	0.1
	D_2	-	0.263		0.4
	D_3	-	-0.349		-1.3
	D_4	-	0.147		0.05
	D_5	-	16.8		0
	$\dot{\varepsilon}_o$	-	1		1×10^{-4}

Table 5-3: Mie-Grüneisen Parameters

Parameter	**Symbol**	**Unit**	**AA5083-H116 [61]**	**Bullet Core [74]**	**Steel Secure 500 [74]**
Grüneisen coefficient	γ	-	1.97	1.93	1.67
Slope values	S	-	1.4	1.49	1.73
Elastic wave velocity	C	m/s	5340	4570	4570

5.5 Modelling of Parts

5.5.1 High Hardness Perforated Plate

Steel Secure 500 is used to manufacture high hardness perforated plate. The plate was quenched and tempered to achieve high hardness properties. Tensile strength of material is 1600 MPa while yield strength is 1300 MPa. Dimensions of plate were 307 x 304 x 8 mm. The size of high hardness perforated plate ensures that waves of stress produced by plate edges do not have any effect on bullet impact.

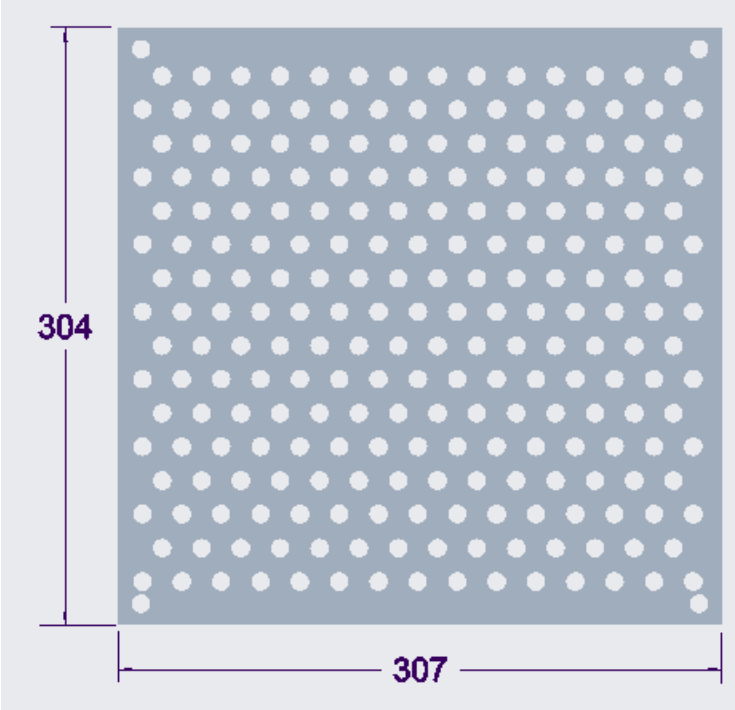

Figure 5.1: High Hardness Perforated Plate with Circular Perforations

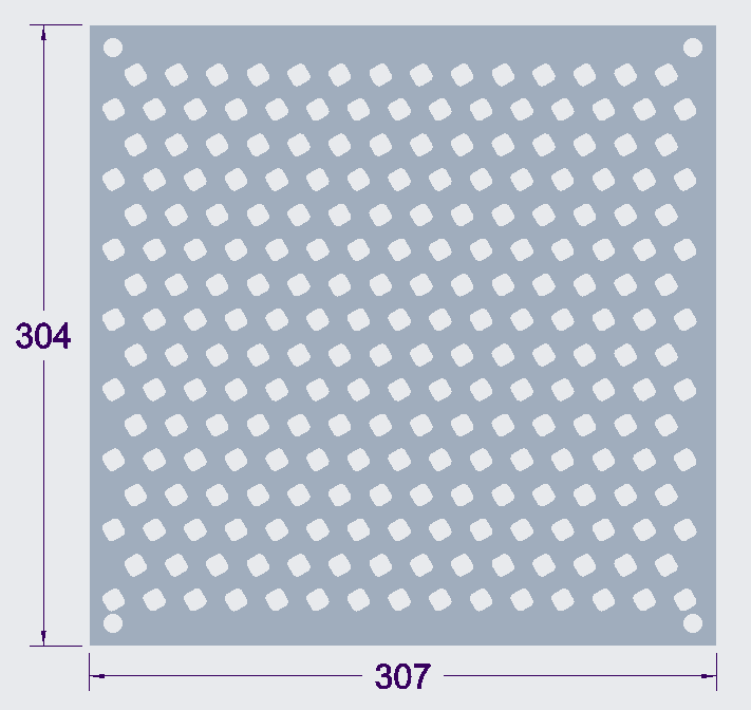

Figure 5.2: High Hardness Perforated Plate with Diamond Shaped Perforations

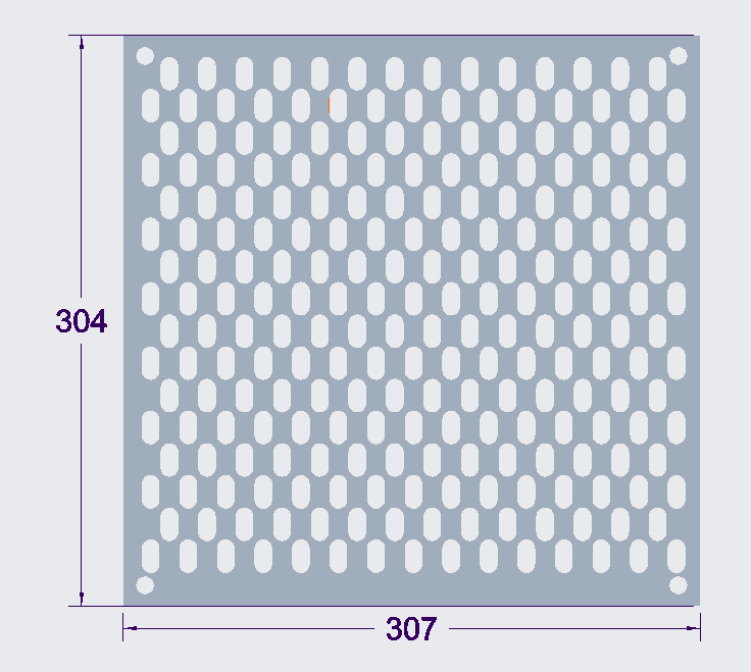

Figure 5.3: High Hardness Perforated Plate with Slot Shaped Perforations

5.5.2 Aluminum AA5083-H116 Base Plate

Aluminum alloy AA5083-H116 was used to manufacture base plate. The mechanical properties of material are given in table 5-1. The dimensions of base plate were 304 x 307 x 38.1 mm.

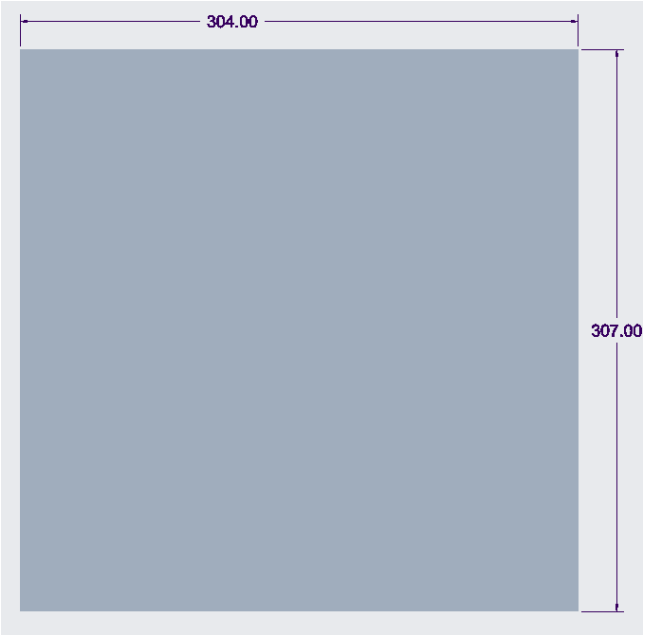

Figure 5.4: Aluminum AA5083-H116 Base Plate

5.5.3 Armor Piercing Projectile

7.62 x 51 mm armor piercing projectile is used in experimentation and numerical analysis. The core of this type of projectile is made up of hardened steel. It has a brass jacket and lead antimony cap. Bullet velocity depends upon powder's quantity in cartridge. The velocity of bullet for these numerical simulations is taken as 891 m/s which is average velocity of experimentation done.

Figure 5.5: 7.62 x 51 mm Armor Piercing Projectile

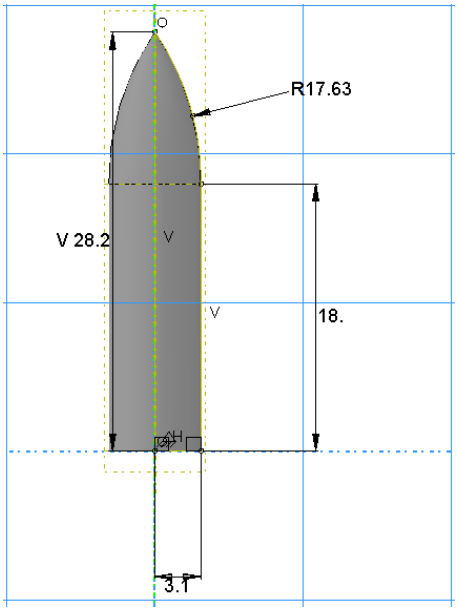

Figure 5.6: Dimensions of 7.62 x 51 mm Armor Piercing Projectile

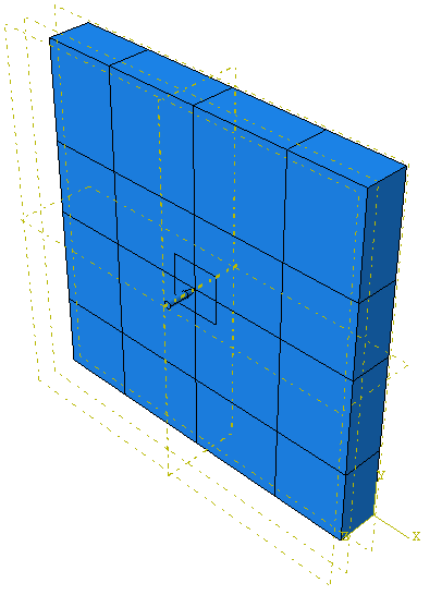

Figure 5.7: Assembly of Case-1: Impact on Base Aluminum Plate

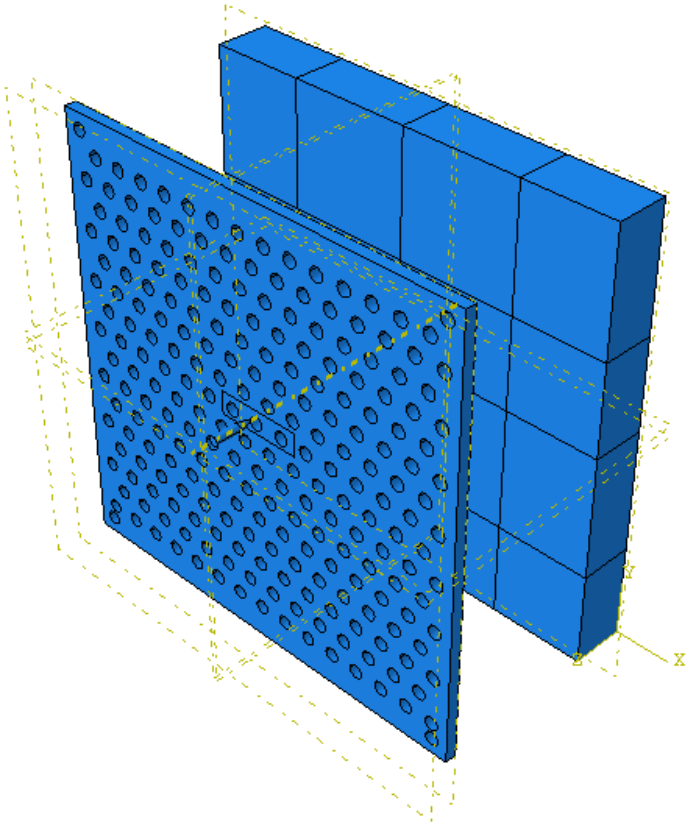

Figure 5.8: Assembly of Case-2: Impact on High Harness Plate with Circular Perforations

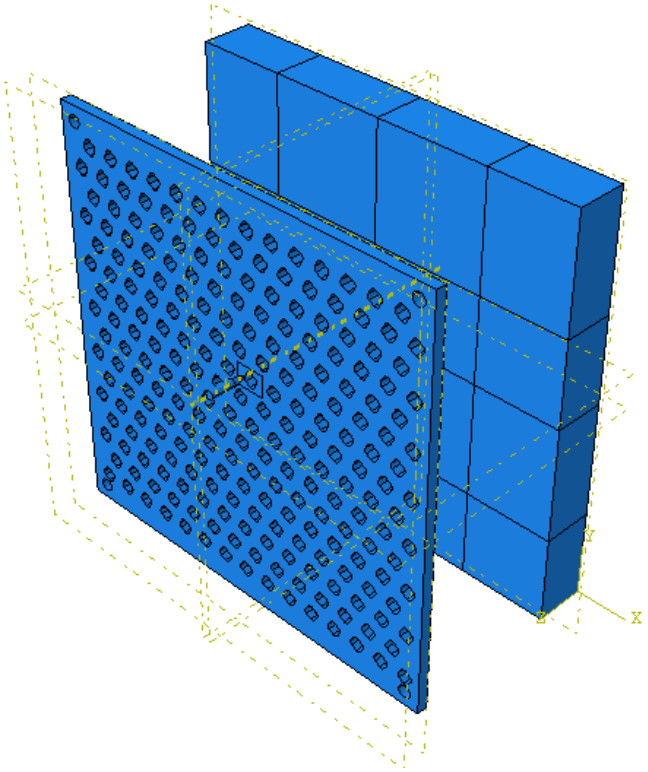

Figure 5.9: Assembly of Case-3: Impact on High Harness Plate with Diamond Shaped Perforations

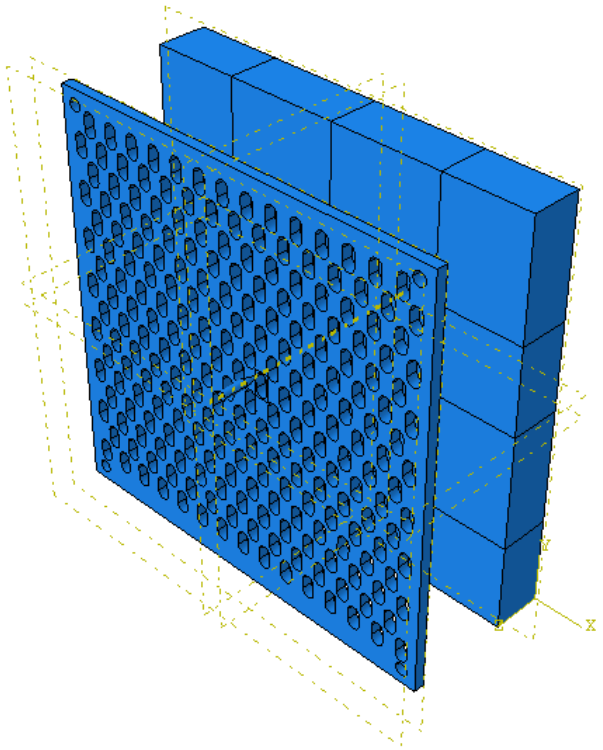

Figure 5.10: Assembly of Case-4: Impact on High Harness Plate with Slot Shaped Perforations

5.6 Mesh for Numerical Analysis

Continuous Mesh, changing from coarse to fine, is utilized in this ballistic impact analysis. Parts were portioned into two parts. The part with interest has very mine meshing while other portion has coarse mesh. These portions are seeded with suitable mesh size to get required refined mesh and continuum behavior in results.

5.6.1 Mesh of Base Armor Plate

8 node linear brick, reduced integration with hourglass control elements (structured mesh) are used to mesh base armor plate using meshing module of Abaqus CAE. The base plate was sectioned into two portions. Element size is selected between 0.6 to 11 mm. The mesh size was finest in region where bullet hits the target. Mesh size increases from target to edge of the plate in every direction.

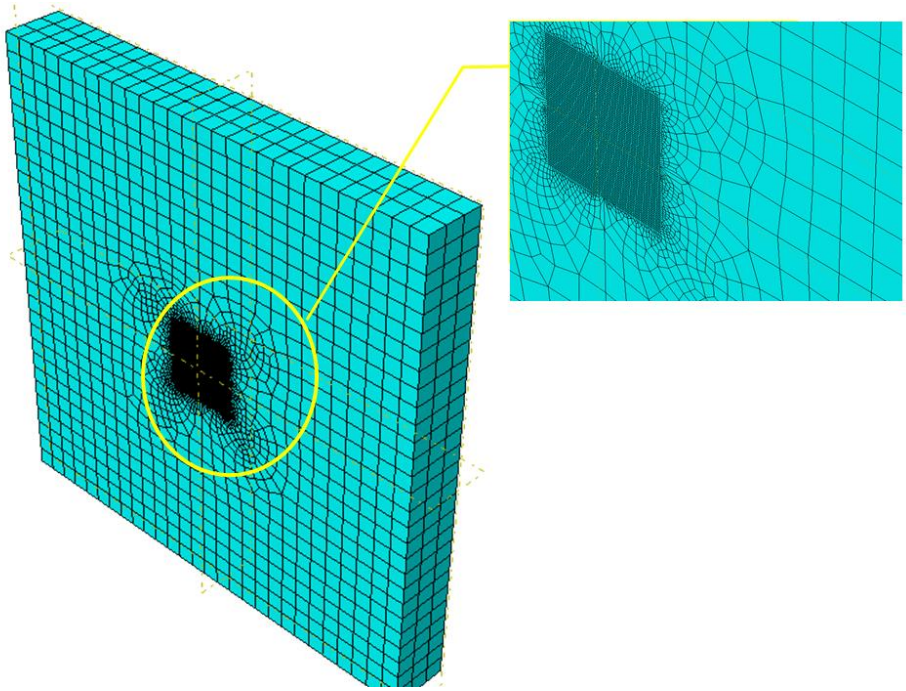

Figure 5.11: Mesh of Base Armor Plate

5.6.2 Mesh of Armor Piercing Projectile

8 node linear brick, reduced integration with hourglass control elements (structured mesh) are used to mesh armor piercing projectile using meshing module of Abaqus CAE. Projectile is not partitioned. Mesh size of 1.5 mm is kept on entire projectile.

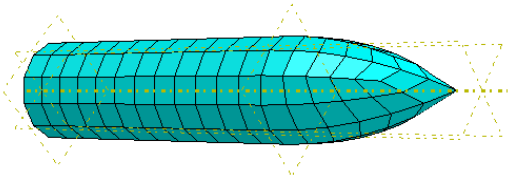

Figure 5.12: Mesh of 7.62 x 51 mm Armor Piercing Projectile

5.6.3 Mesh of High Hardness Perforated Armor Plates

8 node linear brick, reduced integration with hourglass control elements (structured mesh) are used to mesh high hardness perforated armor plate using meshing module of Abaqus CAE. Plates were divided into two regions for ease of meshing. Element size lies between 1 to 15 mm. The portion at which bullet will impact has mesh size of 1 mm.

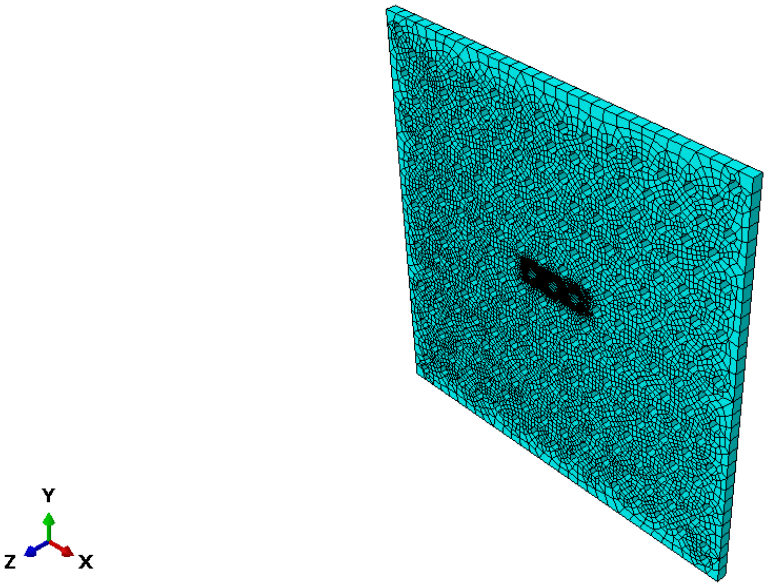

Figure 5.13: Mesh of High Hardness Plate with Circular Perforations

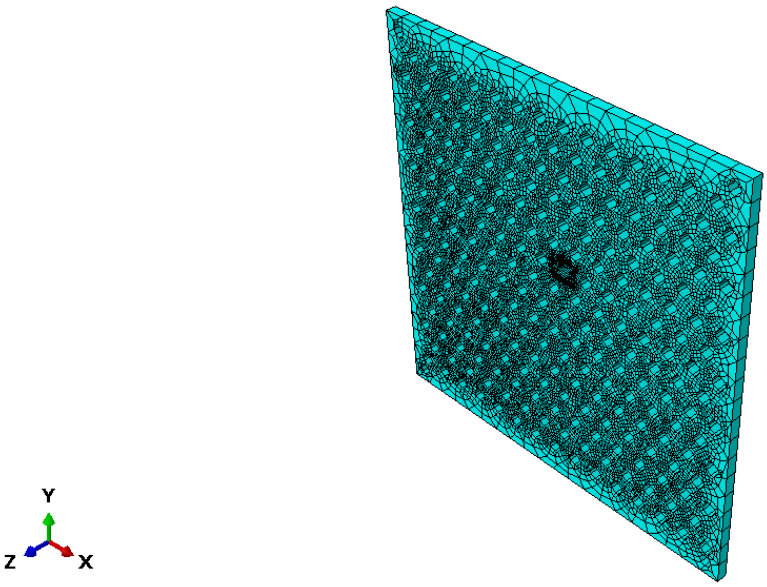

Figure 5.14: Mesh of High Hardness Plate with Diamond Shaped Perforations

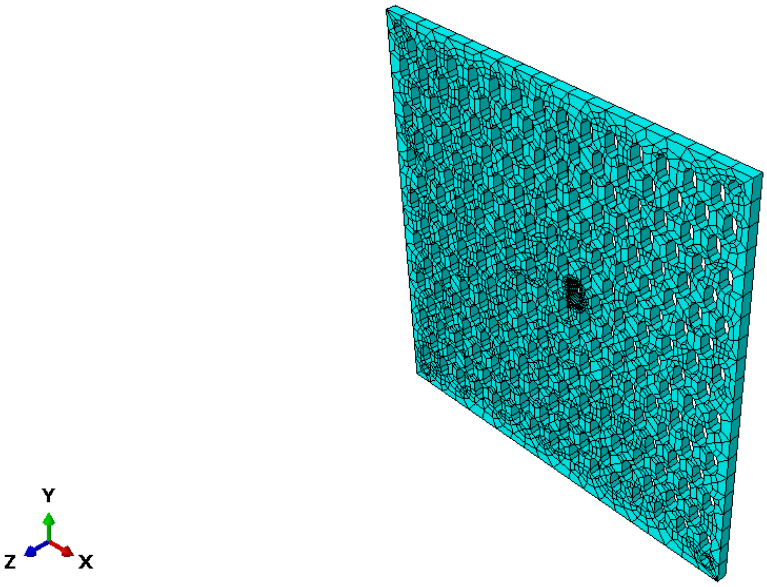

Figure 5.15: Mesh of High Hardness Plate with Slot Shaped Perforations

5.7 Contact

General contact was used between all three parts including projectile, base armor plate and high hardness perforated plate. General contact defines contact between external elements of all surfaces. To get both internal and external contact, surfaces of all parts were edited using SciTex editor. Frictionless interaction was deployed between parts of assembly. To improve results of analysis, adiabatic effects were also included.

CHAPTER 6: RESULTS AND DISCUSSION

6.1 Case-1 (Monolithic Aluminum Base Plate Only)

It was shown by experiments that 7.62 x 51mm AP hard core bullet penetrated through Aluminum AA5083-H116 base plate as shown in figure 6.1. The projectile completely perforated 38.1 mm Aluminum AA5083-H116 base plate. Figure 6.2 depicts High Speed Camera versus time perforation of AP projectile.

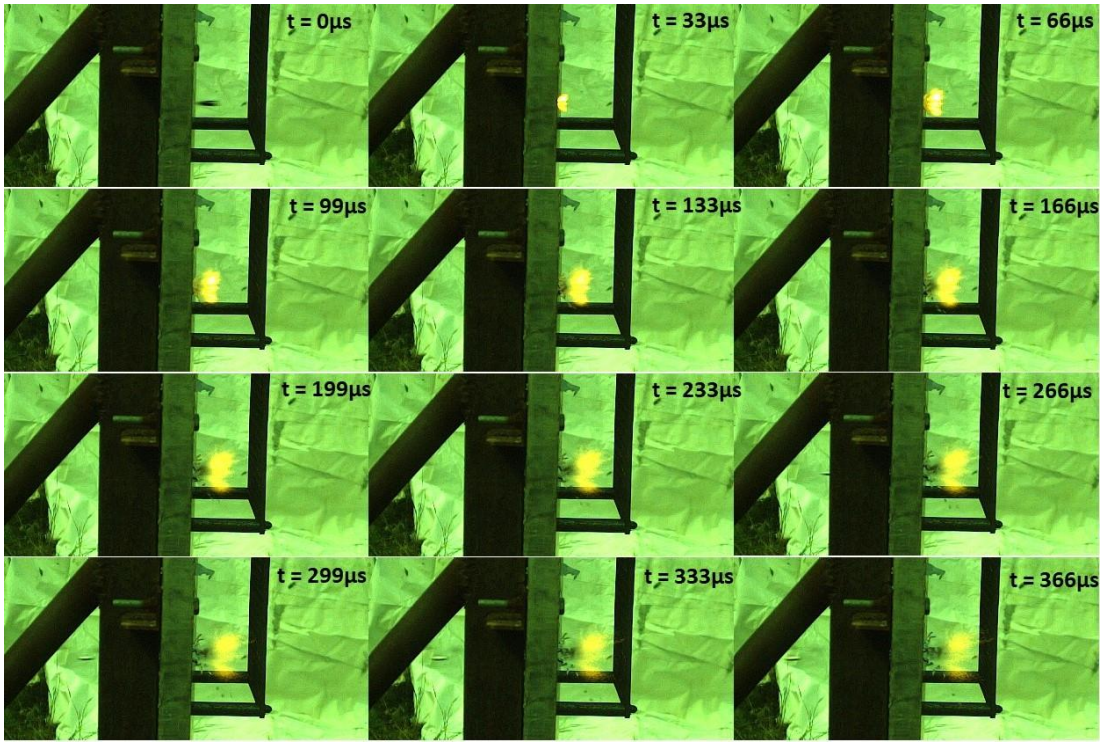

Figure 6.1: High Speed Camera versus time depicting perforation of 7.62 x 51 mm AP Hard Core bullet through Monolithic Aluminum Base Plate

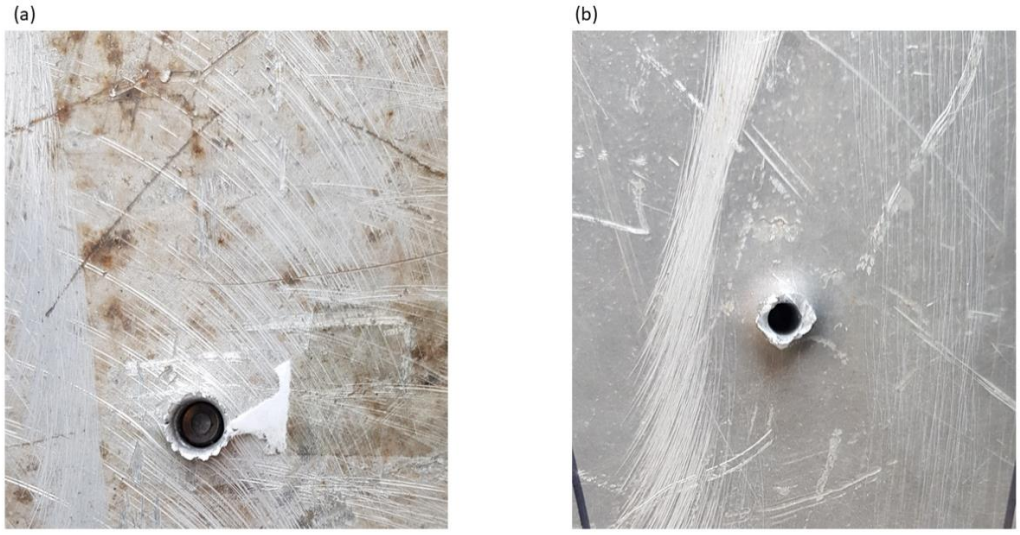

Figure 6.2: Base Armor Plate showing impact of 7.62 x 51 mm AP Hard Core Bullet (a) Impact Side (b) Distal Side

Experimental data is compared to numerical analysis. The ballistic progression of perforation of 7.62 x 51 mm hard core armor piercing projectile is shown in figure 6.3 below. The penetration pattern in numerical analysis and experiments is much similar to each other

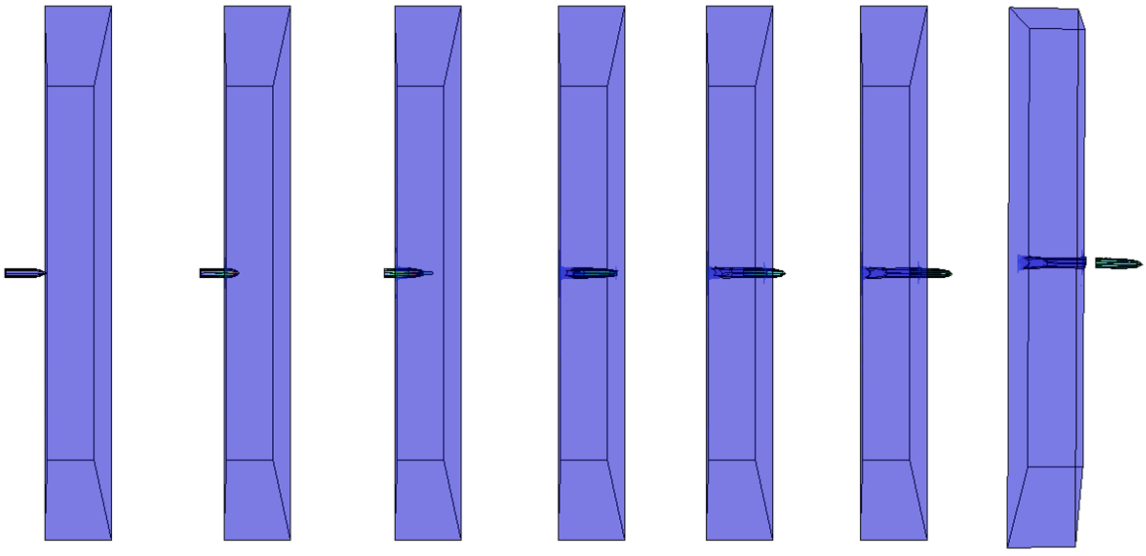

Figure 6.3: Analysis Progression in 38.1 mm Base Armor Plate

Figure 6.4 shows internal energy and kinetic energy versus time graph of complete assembly. The kinetic energy of bullet starts declining and internal energy starts growing when

projectile hits 38.1 mm thick Aluminum AA5083-H116 base armor plate. Larger amount of internal energy absorbed by base armor plate, better will be the base armor plate's resistance against projectile.

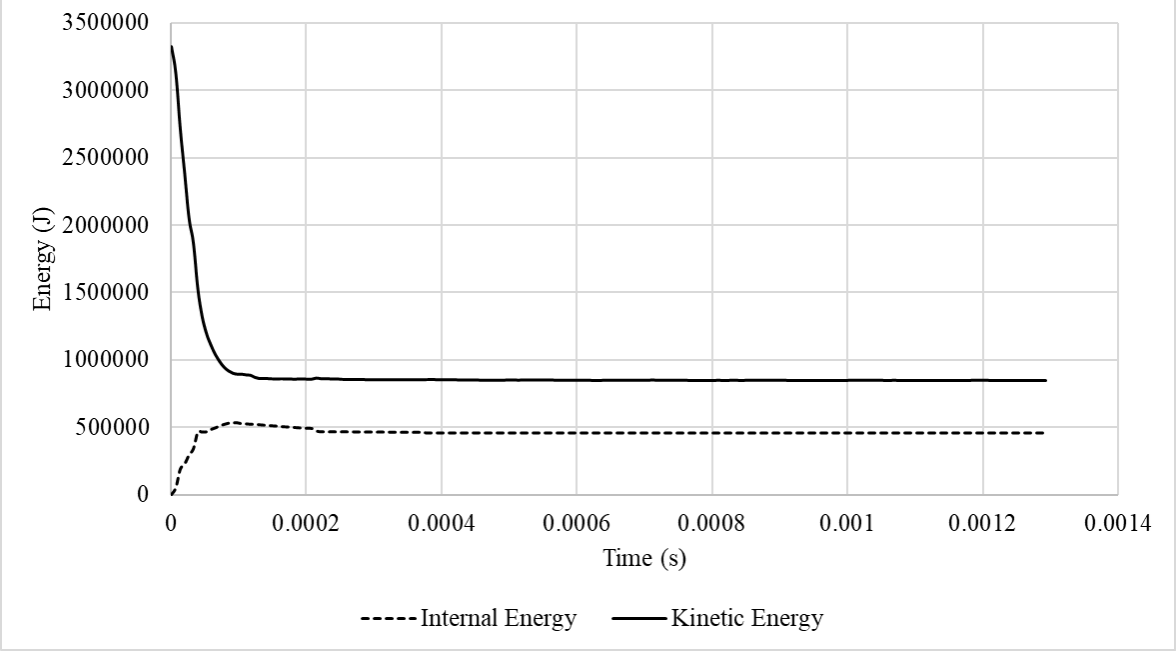

Figure 6.4: Kinetic Energy and Internal Energy vs Time for Base Armor Plate

The base armor plate will resist armor piercing projectiles as long as projectile's kinetic energy is equal or greater than internal energy of base armor plate. Even after armor plate's failure, kinetic energy is still remaining in the projectile.

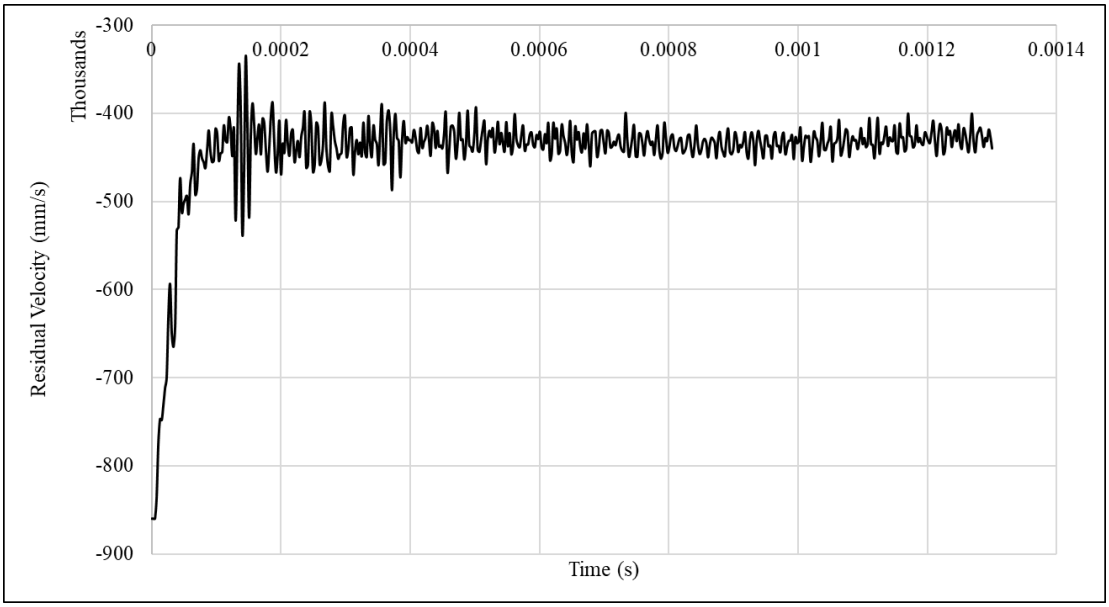

Figure 6.5: Residual Velocity vs Time for Base Armor Plate

6.2 Case-2 (Base Plate Fitted Steel Plate with Circular Perforations)

03 rounds of 7.62 x 51 mm AP Hard Core Projectile were fired on Base plate when fitted with high Hardness Steel Plate with circular perforations. The high hardness steel plate was able to stop all these projectiles (Figure 6.3). Figure 6.4 depicts projectile impacting on perforated plate then on base plate. The core was not shattered but penetrated partially into the base plate. No traumas were formed on the distal side of base armor plate.

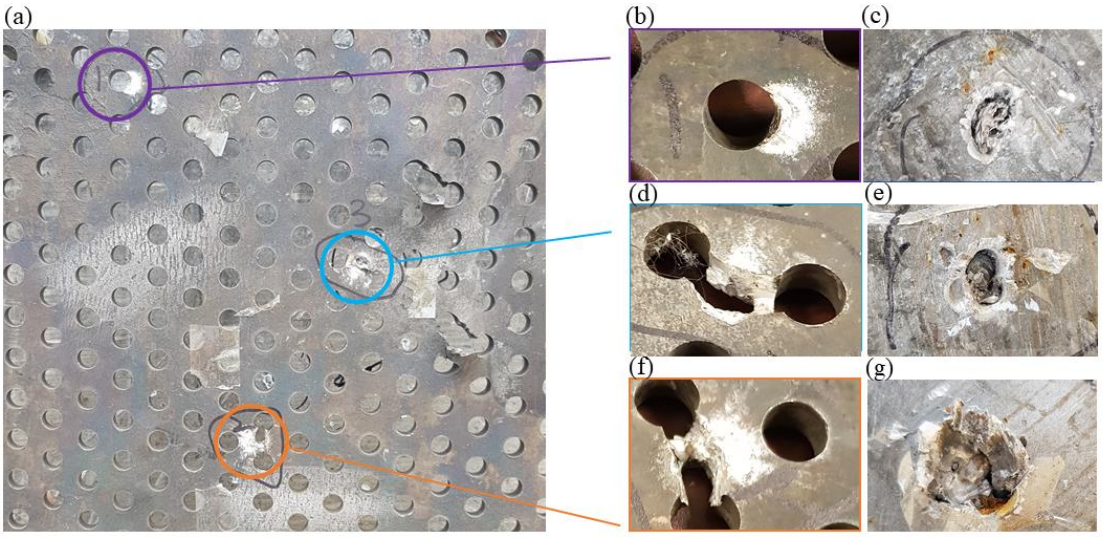

Figure 6.6: High Hardness Steel Plate with Circular Perforations showing impact of 7.62 x 51 mm AP Hard Core Bullet (a) Impact Side (b) Zoomed view of 1st Shot on Impact Side (c) Zoomed View of 1st Shot on Base Armor Plate (d) Zoomed view of 3rd Shot on Impact Side (e) Zoomed View of 3rd Shot on Base Armor Plate (f) Zoomed view of 2nd Shot on Impact Side (g) Zoomed View of 2nd Shot on Base Armor Plate

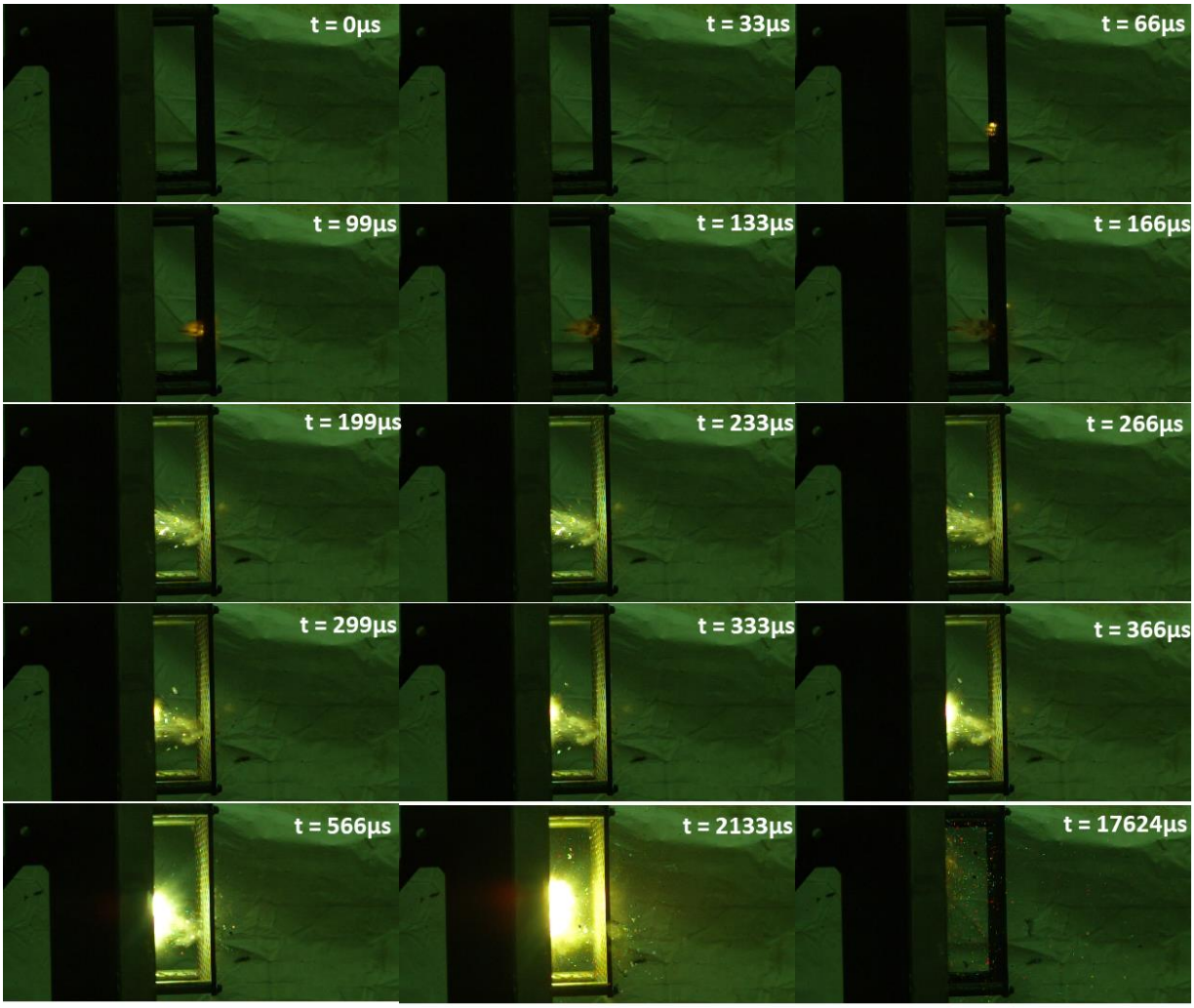

Figure 6.7: High Speed Camera versus time depicting impact of 7.62 x 51 mm AP Hard Core bullet on High Hardness Steel Plate with Circular Perforations

Ballistic progression of impact of 7.62 x 51 mm hard core armor piercing projectile on high hardness perforated plate at initial velocity of 891 m/s is illustrated in figure 6.8. The simulation shows that projectile is fractured by high hardness perforated plate and trajectory of projectile is also changed. This helps base armor plate to stop the projectile. Kinetic energy decreases rapidly after the impact while internal energy increases. A great amount of energy is absorbed by perforated plate which reduces the impact of projectile on base armor. After failure of high hardness perforated plate, a minute amount of kinetic energy still remains in projectile. This causes projectile to penetrate a few millimeters into the base armor as shown in figure below.

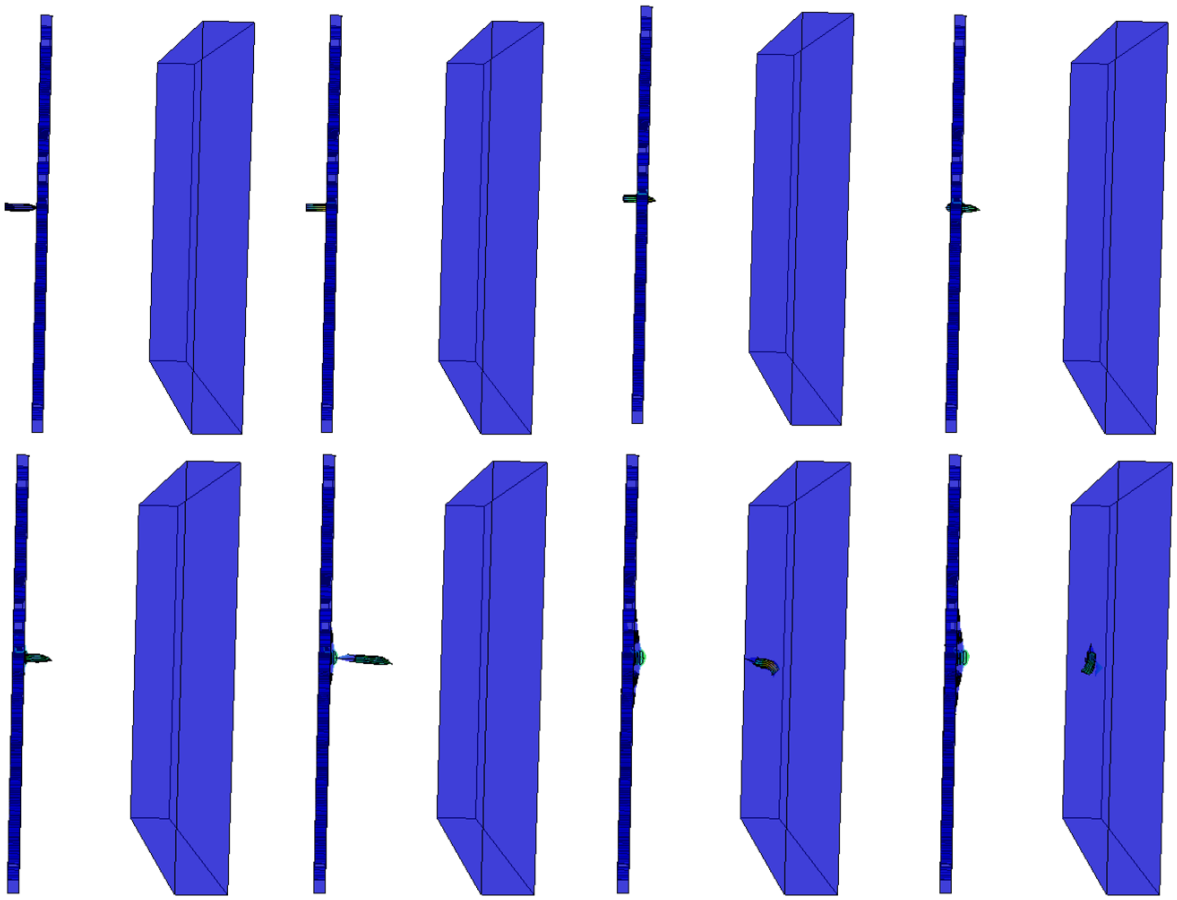

Figure 6.8: Analysis Progress in High Hardness Plate with Circular Perforation

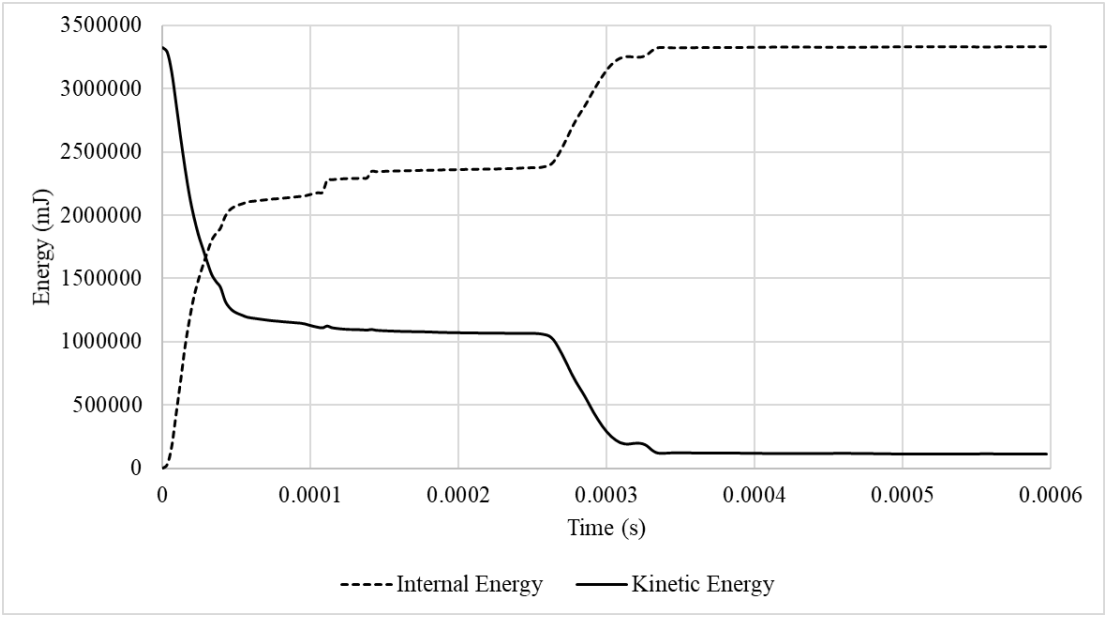

Figure 6.9: Kinetic Energy and Internal Energy vs Time for High Hardness Plate with Circular Perforation

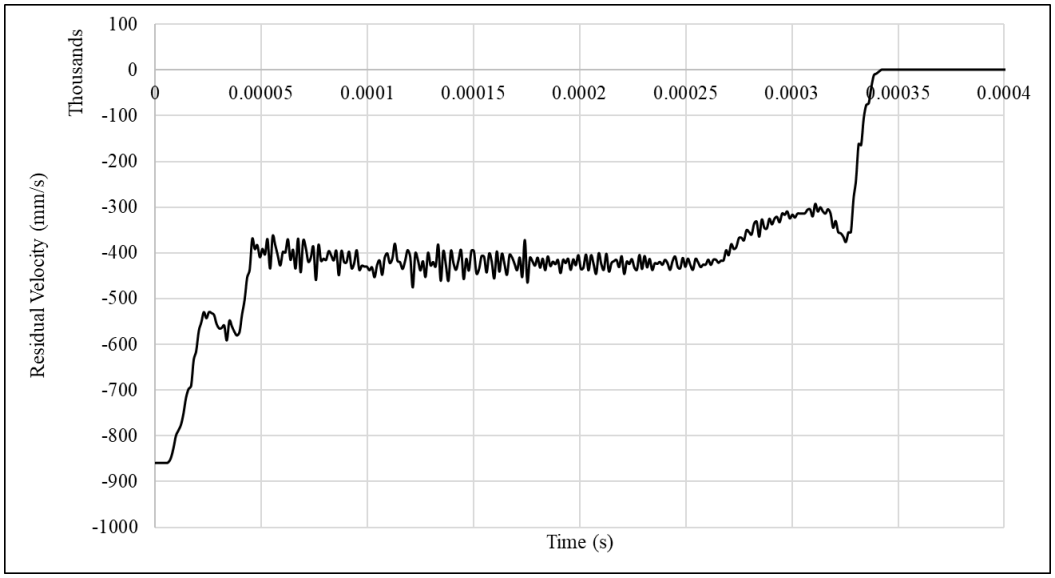

Figure 6.10: Residual Velocity vs Time for High Hardness Plate with Circular Perforation

6.3 Case-3 (Base Plate Fitted Steel Plate with Diamond Shaped Perforations)

The high hardness steel plate with diamond shaped perforations deflected AP hard core projectiles from their original path as visualized in Figure 6.5. In this case, core was shattered in 1st and 2nd Shot while penetrated partially in 3rd shot (Figure 6.6). No traumas were formed on the distal side of base armor plate.

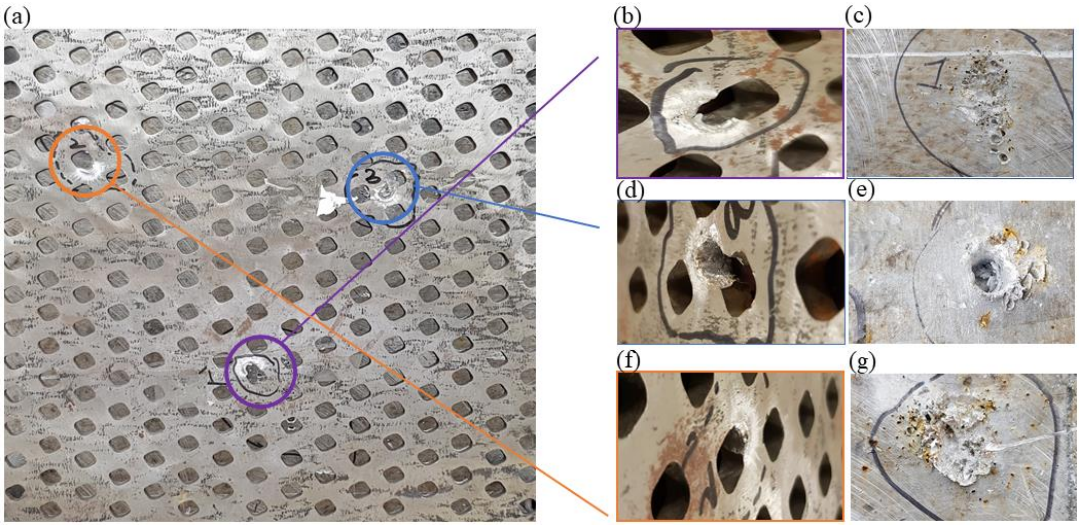

Figure 6.11: High Hardness Steel Plate with Diamond Shaped Perforations showing impact of 7.62 x 51 mm AP Hard Core Bullet (a) Impact Side (b) Zoomed view of 1st Shot on Impact Side (c) Zoomed View of 1st Shot on Base Armor Plate (d) Zoomed view of 3rd Shot on Impact Side

(e) Zoomed View of 3rd Shot on Base Armor Plate (f) Zoomed view of 2nd Shot on Impact Side (g) Zoomed View of 2nd Shot on Base Armor Plate

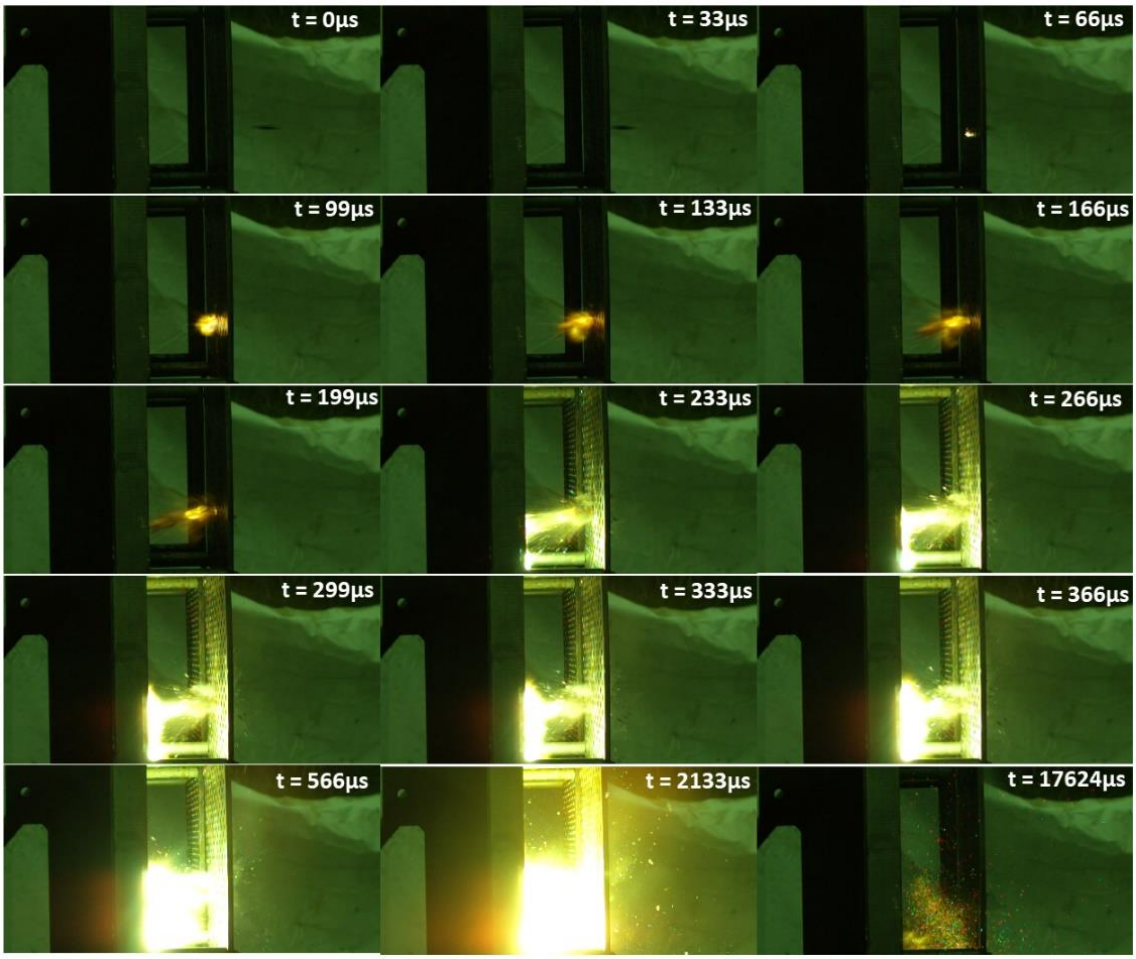

Figure 6.12: High Speed Camera versus time depicting impact of 7.62 x 51 mm AP Hard Core bullet on High Hardness Steel Plate with Diamond Shaped Perforations

Figure 6.13 illustrates ballistic progression of impact of 7.62 x 51 mm hard core armor piercing projectile on high hardness perforated plate with diamond shaped perforations at initial velocity of 891 m/s. The simulation shows that projectile is fractured by high hardness perforated plate and trajectory of projectile is also changed. This helps base armor plate to stop the projectile. Kinetic energy decreases rapidly after the impact while internal energy increases. A great amount of energy is absorbed by perforated plate which reduces the impact of projectile on base armor. After failure of high hardness perforated plate, a minute amount of kinetic energy still remains in projectile. This causes projectile to penetrate a few millimeters into the base armor as shown in figure below.

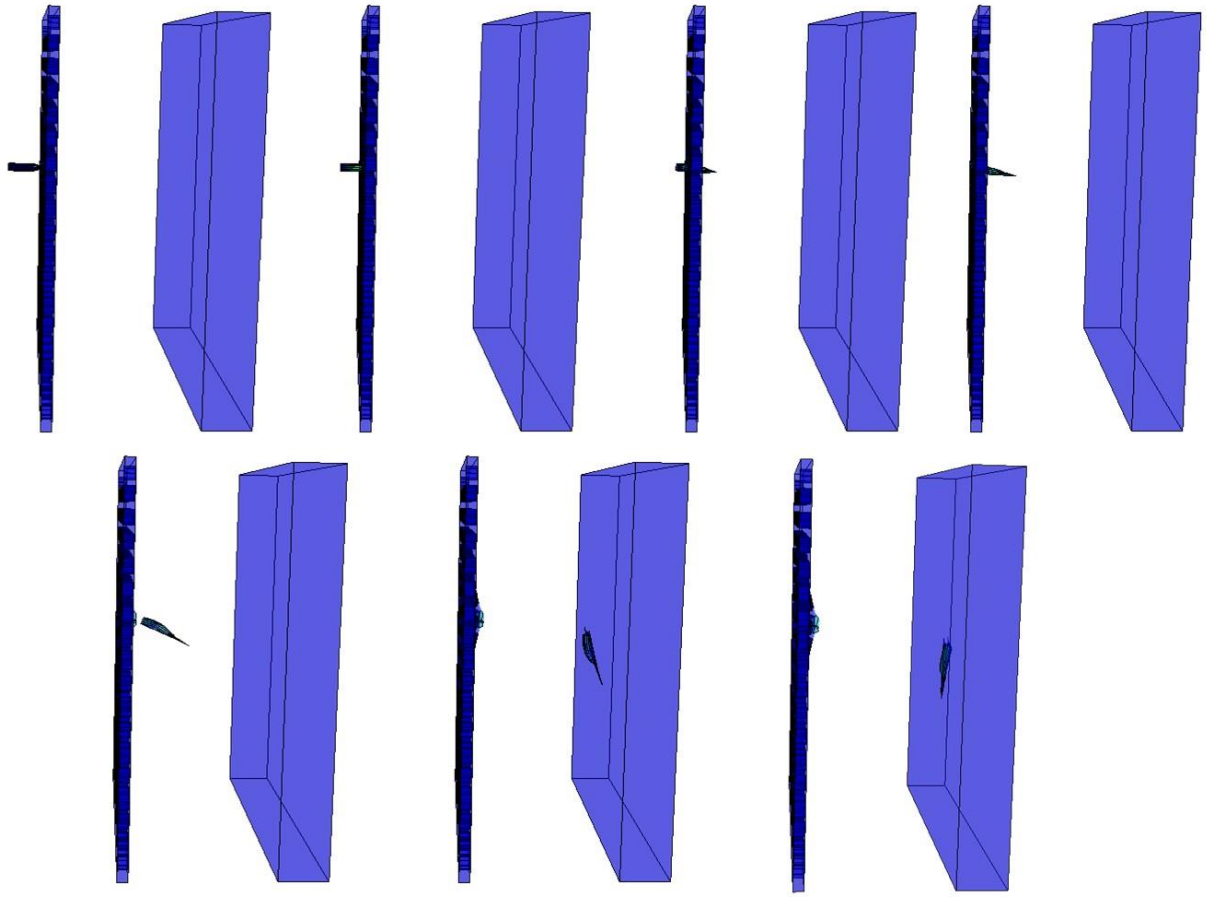

Figure 6.13: Analysis Progression in High Hardness Plate with Diamond Shaped Perforation

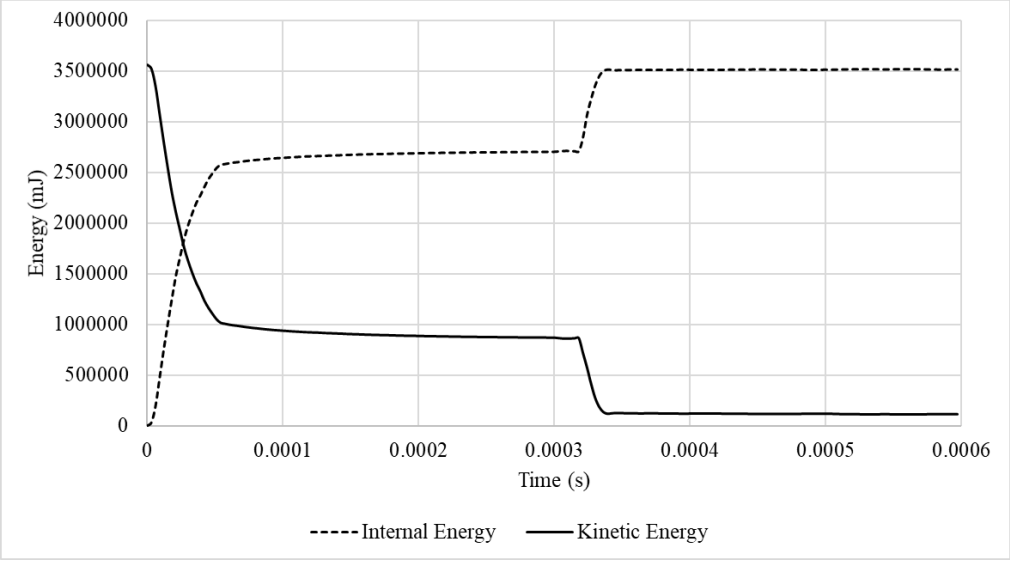

Figure 6.14: Kinetic Energy and Internal Energy vs Time for High Hardness Plate with Diamond Shaped Perforation

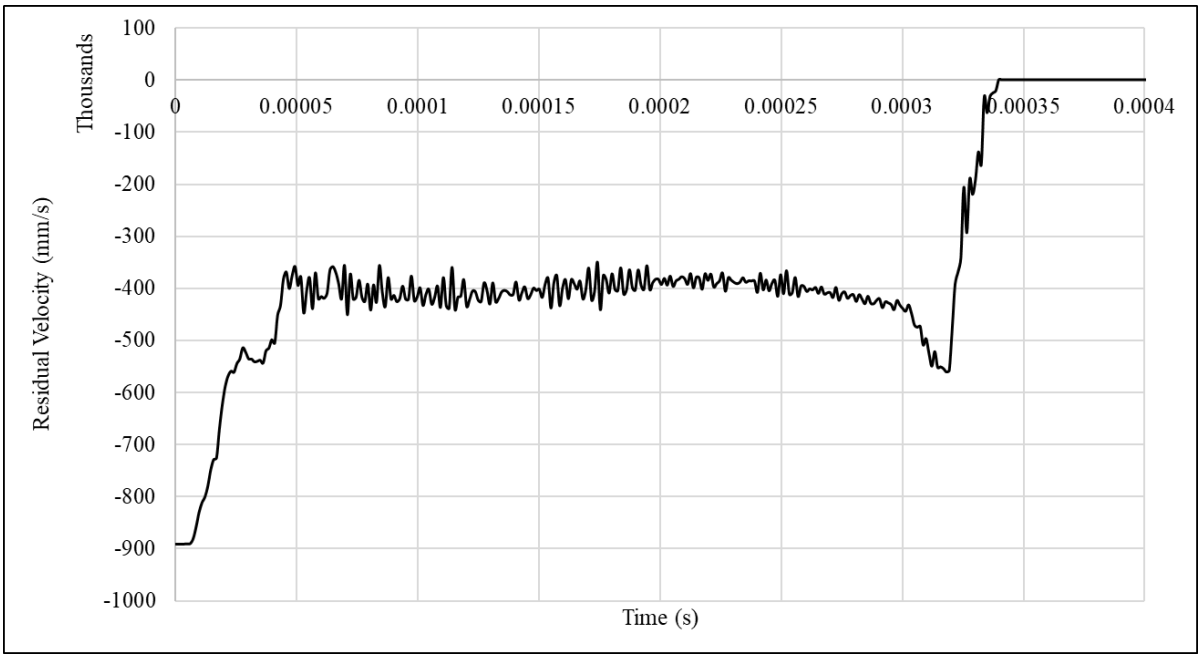

Figure 6.15: Residual Velocity vs Time for High Hardness Plate with Diamond Shaped Perforation

6.4 Case-3 (Base Plate Fitted Steel Plate with Slot Shaped Perforations)

The high hardness steel plate with slot shaped perforations also deflected AP hard core projectiles from their original path as visualized in Figure 6.16. In this case, core penetrated partially in all 3 shots (Figure 6.17). No traumas were formed on the distal side of base armor plate.

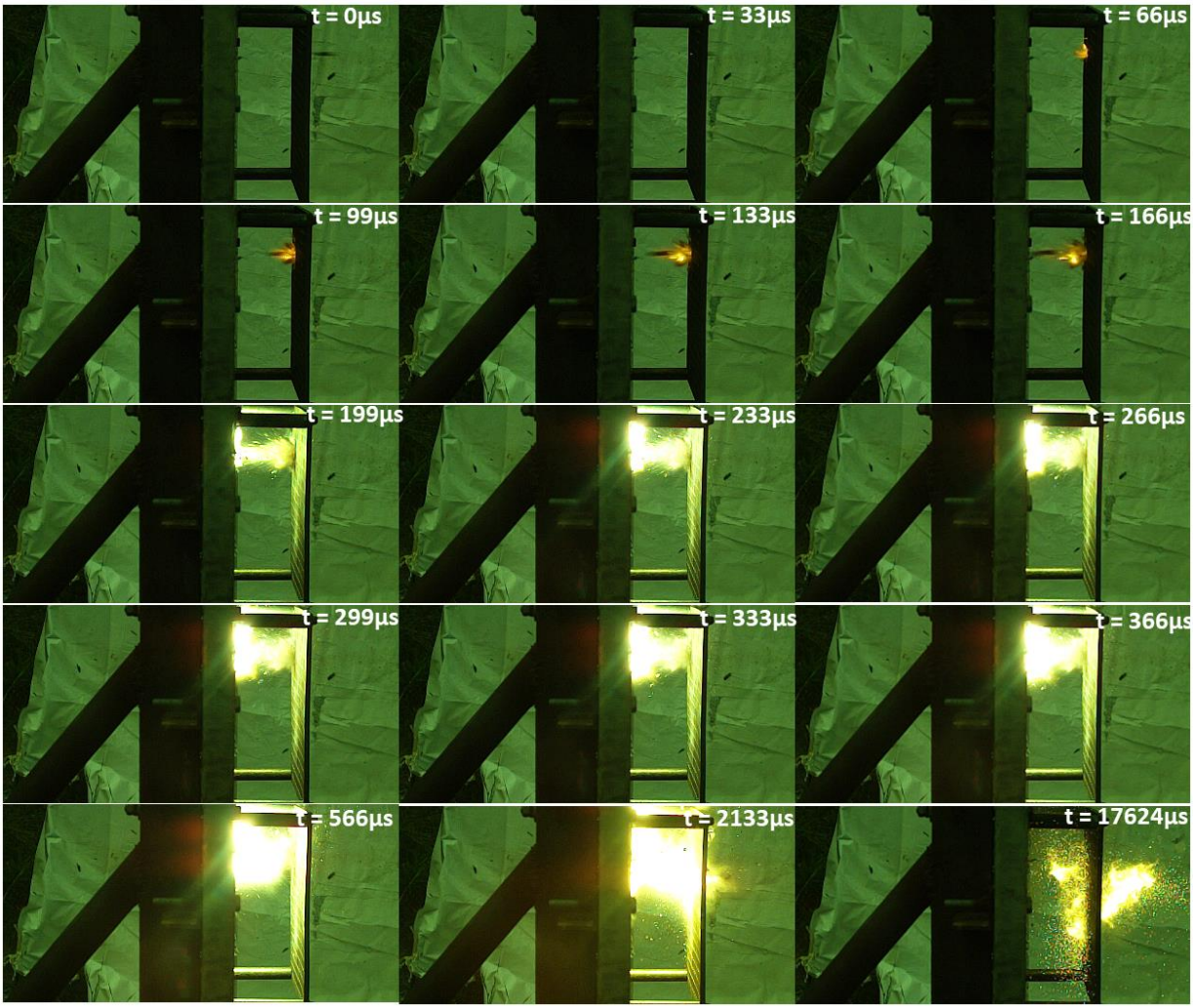

Figure 6.16: High Speed Camera versus time depicting impact of 7.62 x 51 mm AP Hard Core bullet on High Hardness Steel Plate with Slot Shaped Perforations

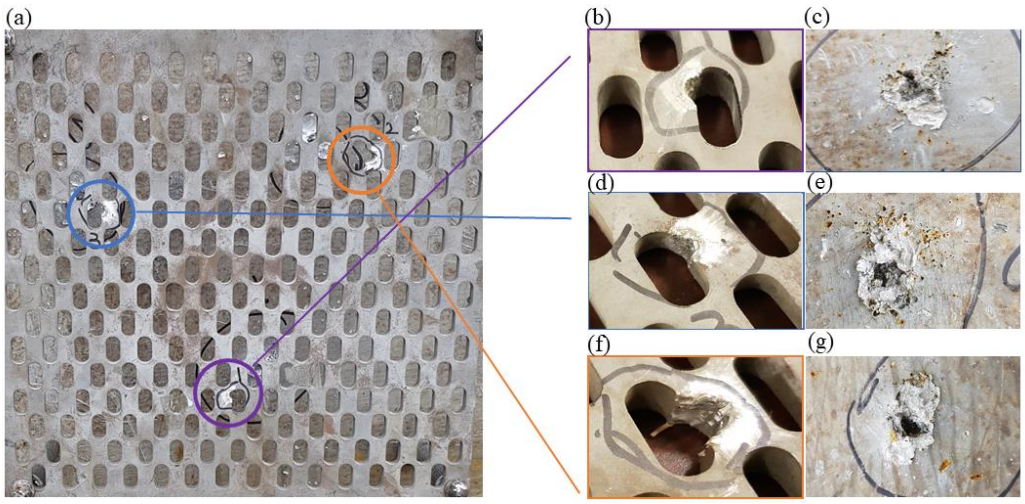

Figure 6.17: High Hardness Steel Plate with Slot Shaped Perforations showing impact of 7.62 x 51 mm AP Hard Core Bullet (a) Impact Side (b) Zoomed view of 1st Shot on Impact Side (c) Zoomed View of 1st Shot on Base Armor Plate (d) Zoomed view of 3rd Shot on Impact Side (e) Zoomed View of 3rd Shot on Base Armor Plate (f) Zoomed view of 2nd Shot on Impact Side (g) Zoomed View of 2nd Shot on Base Armor Plate

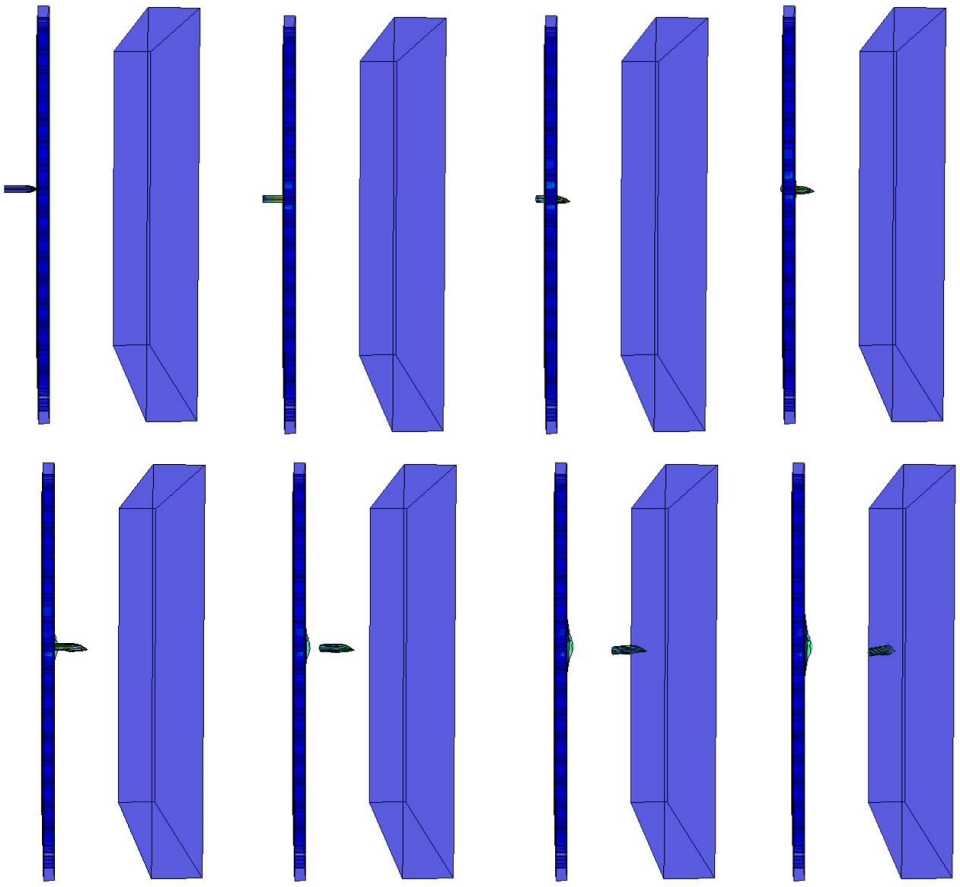

Figure 6.18: Analysis Progression in High Hardness Plate with Slot Shaped Perforation

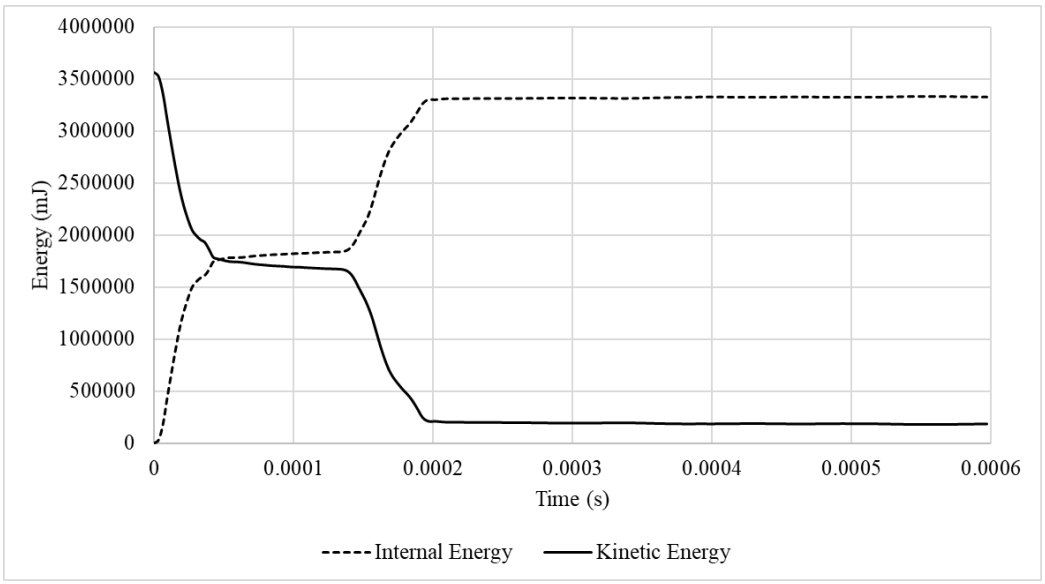

Figure 6.19: Kinetic Energy and Internal Energy vs Time for High Hardness Plate with Slot Shaped Perforations

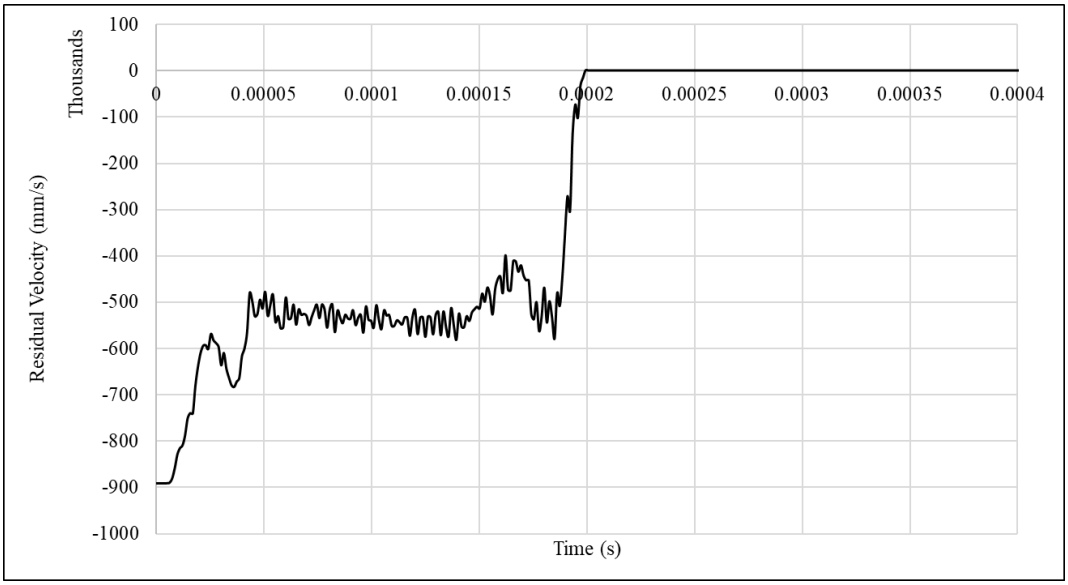

Figure 6.20: Residual Velocity vs Time for High Hardness Plate with Slot Shaped Perforation

The back side of Aluminum armor base plate can be seen in Figure 6.21.

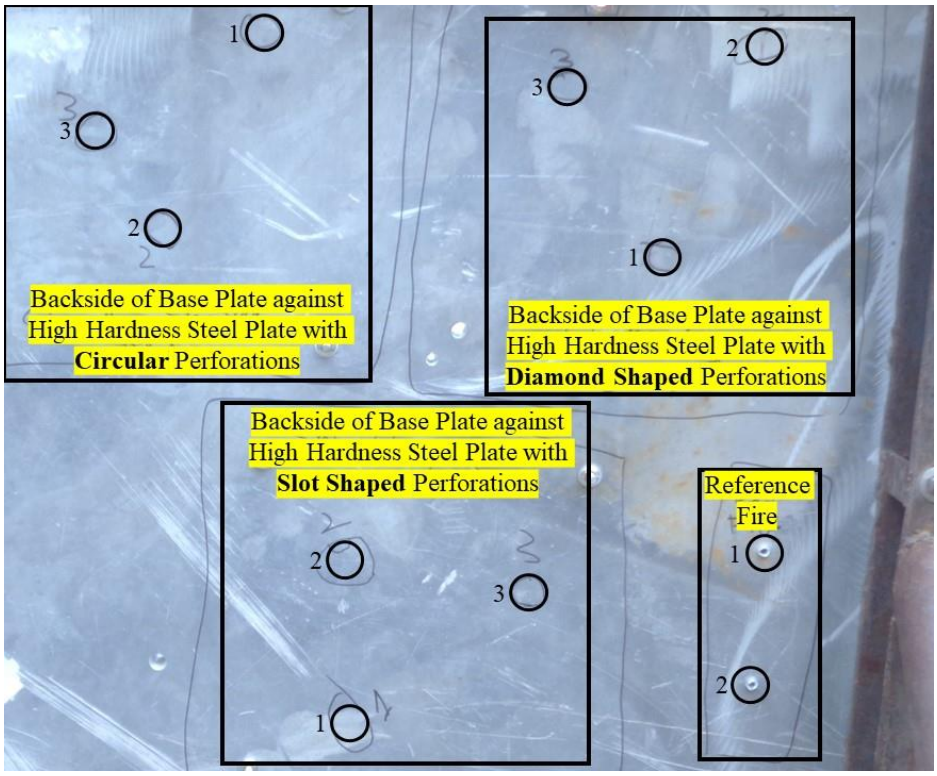

Figure 6.21: Distal Side of Base Plate after experiment

Table 6-1 presents depth of projectile penetration in each case. It can be observed that maximum average depth is found in case-4 i.e., Base Plate Fitted Steel Plate with Slot Shaped Perforations.

Table 6-1: Depth of Penetration of Projectiles in all Cases

	Depth (mm)		
	1st Shot	**2nd Shot**	**3rd Shot**
Base Plate with High Hardness Steel Plate with Circular Perforations	3.1	3.1	3.8
Base Plate with High Hardness Steel Plate with Diamond Shaped Perforations	5.10	8.84	4.25
Base Plate with High Hardness Steel Plate with Slot Shaped Perforations	4	3.2	5.5

7.62 x 51 mm Armor Piercing Hard Core Projectiles completely penetrated the aluminum AA5083-H116 Base Plate when no high hardness steel plate was fitted. The subsequent through holes can be visualized in figure 6.2. Material swelling was observed on impact side of base plate while on the distal side, lip formation was observed. The ductile hole growth was observed in the base armor plate. The fracture in material was localized. The plate is treated as thick target because H/D ratio is 5. Any target plate with H/D ratio greater than 1 is a thick target when "H" is thickness of target plate while "D" is diameter for projectile to be fired [81]. When High Hardness Steel Plate with perforations were fitted on the aluminum base plate, the AP hard core projectile penetrated the high hardness steel plate while it was incapable to pierce the base plate, as visualized in figure 6.7, 6.12 and 6.17. The AP hard core projectile partly overlaid the perforations on high hardness steel plate to create edge effect. In case of high hardness plate with circular perforations, a brittle fracture was observed and connection between perforations were broken as illustrated in figure 6.7. In case of other two high hardness steel plates i.e., Diamond Shaped and Slot Shaped, also brittle fracture was detected but ligaments between perforations were not broken due to comparatively larger size of perforation in these plates. The fragments and other parts of projectile were captured by aluminum base plate. Different depths of carter were observed on the base plate as it depends upon the point of impact of projectile and its interaction with the base plate. Same could be observed in figure 6.7, 6.12 and 6.17. The variations in penetration depth of projectile in base plate was due to generation of random sized fragments upon disintegration of the AP hard core projectile. A transition range of failure mechanism change from adiabatic shear to Projectile breakup is present at hardness of 500 HB for steels [82]. It can be seen, as high hardness steel plates are of 550HB that the projectile breakup along with change in path of fragments due to impact on edge of perforation may become the dominated defeating mechanism. After impact with the high hardness steel plate, the projectile diverged from its original path.

6.5 Mass Effectiveness

Frank developed mass effectiveness factor to evaluate ballistic performance of an armor material [83]. Mass Effectiveness (E_m) is comparative measure of areal mass of armor material to be evaluated required to defeat a threat, relative to areal mass of a traditional armor such as Rolled Homogeneous Armor steel (RHA) and High Hardness Aluminum required to defeat the identical threat. It can be defined as:

$$E_m = \frac{\rho_o \times t_o}{\rho \times t} \quad (13)$$

Where ρ_o and t_o are density and thickness of reference traditional armor material required to defeat the projectile while ρ and t are density and thickness of armor material to be evaluated required to defeat the same projectile. In this research, the projectile was 7.62 x 51 mm AP hard core bullet. Military Specification for Rolled Homogenous Armor are given in MIL-A-12560A [17]. As per MIL-A-12560A, a 17.323 mm thick Rolled Homogeneous Armor Plate should stop a 7.62 x 51 mm armor piercing projectile moving at a speed of 891 m/s. Mass Effectiveness factor keeping thickness of Aluminum Al 5083-H116 same as of monolithic base plate is given in Table 6-2. The Mass Effectiveness factor can be increased by reducing thickness of Aluminum Al 5083-H116 to 20 mm because none of the projectile made carter greater than 8 mm with an average of 5 mm. Increased mass effectiveness factor can be seen in Table 6-3. In table 6-2 and 6-3, comparison is drawn using Rolled Homogeneous Armor as reference material. Same comparison can be drawn using military specification "MIL-A-46027" for Aluminum Alloy Armor [84]. As per MIL-A-46027, a 54.34 mm Aluminum Armor Plate Al 5083-H116 should stop a 7.62 x 51 mm armor piercing projectile moving at a speed of 891 m/s. Table 6-4 and 6-5 provides mass effectiveness keeping thickness of Aluminum Al 5083-H116 same as of monolithic base plate and with reduced thickness of Aluminum Al 5083-H116 to 20 mm.

Table 6-2: Mass Effectiveness in comparison of Rolled Homogeneous Armor

	Density	**Thickness**			
RHA	7850	0.01732			
	Density of Perforated Plate	**Thickness of Perforated Plate**	**Density of AA5083-H116**	**Thickness of AA5083-H116**	**Mass Effectiveness**
Case 2	7850	0.008	2700	0.0381	0.821
Case 3	7850	0.008	2700	0.0381	0.821
Case 4	7850	0.008	2700	0.0381	0.823

Table 6-3: Mass Effectiveness in comparison of Rolled Homogeneous Armor with reduced thickness AA5083-H116

	Density	**Thickness**			
RHA	7850	0.01732			
	Density of Perforated Plate	**Thickness of Perforated Plate**	**Density of AA5083-H116**	**Thickness of AA5083-H116**	**Mass Effectiveness**
Case 2	7850	0.008	2700	0.02	1.164
Case 3	7850	0.008	2700	0.02	1.164

Case 4	7850	0.008	2700	0.02	1.164

Table 6-4: Mass Effectiveness in comparison of 38.1 mm Aluminum AA5083-H116 Armor

	Density	**Thickness**			
AA5083-H116	2700	0.05434			
	Density of Perforated Plate	**Thickness of Perforated Plate**	**Density of AA5083-H116**	**Thickness of AA5083-H116**	**Mass Effectiveness**
Case 2	7850	0.008	2700	0.0381	0.886
Case 3	7850	0.008	2700	0.0381	0.886
Case 4	7850	0.008	2700	0.0381	0.886

Table 6-5: Mass Effectiveness in comparison of 20 mm thick Aluminum AA5083-H116 Armor

	Density	**Thickness**			
AA5083-H116	2700	0.05434			
	Density of Perforated Plate	**Thickness of Perforated Plate**	**Density of AA5083-H116**	**Thickness of AA5083-H116**	**Mass Effectiveness**
Case 2	7850	0.008	2700	0.02	1.256
Case 3	7850	0.008	2700	0.02	1.256
Case 4	7850	0.008	2700	0.02	1.256

The mass effectiveness factor is greater than 1 in Table 6-3 and 6-5 which depicts better performance of armor systems. The mass of each high hardness perforated plate is given in table 6-6:

Table 6-6: Mass of High Hardness Perforated Armor Plates

	Case-2 Plate with Circular Perforations	**Case-3 Plate with Diamond Shaped Perforations**	**Case-4 Plate with Slot Shaped Perforations**
Mass (Kgs)	4.641	4.489	3.543

High hardness armor plate with slot shaped perforations has lowest mass with same mass effectiveness as other two cases under consideration.

CHAPTER 7: CONCLUSION

Performance of Aluminum AA5083-H116 armor plate with additional high hardness perforated armor plate is studied in this research using experimental and computational techniques. Figure 6.1 shows high-speed camera video of 7.62 x 51 mm armor piercing round passing through 38.1 mm thick Aluminum AA5083-H116 armor plate while figure 6.3 shows the simulation of same using Johnson-Cook Failure Criteria. It can be observed in figure 6.4, that internal energy of system rises while kinetic energy declines swiftly. The failure of 38.1 mm thick Aluminum AA5083-H116 armor plate occurs when strain energy absorption capacity is touched. The residual kinetic energy helps bullet to perforate through the base plate as shown in figure 6.1 and 6.3. The high-speed camera footage and numerical simulation results are very similar to each other which increases reliability of simulation results. Numerical analysis has captured reliable and useful details for determining interaction of 7.62 x 51 mm armor piercing projectile with aluminum AA5083-H116 base plate. Minimum thickness required to stop 7.62 x 51 mm armor piercing projectile is 54.34 mm. It is not practical to use 55 – 65 mm thick plate to stop armor piercing projectile. That is why an alternative protection method is requires to strengthen protection capacity of aluminum AA5083-H116.

An 8 mm thick high hardness perforated steel plate was used to protect aluminum AA5083-H116 base plate. It was depicted by experiments that high hardness perforated steel plate squashes steel core of armor piercing projectile which decreases bullet penetration through aluminum base plate. The perforated armor plate diverges path of bullet. Bending of bullet because of high strain energy applied by perforated armor plate causes diversion in path of projectile. This deviation of path is modelled in simulation as well as shown in high-speed camera footage. The penetration depth in simulation is also similar to that found in experiments (3~5 mm approximately). But path deviation is not the only reason behind projectile failure.

The usage of failure criteria for projectile reduces perforation capability of the bullet core. The results are much similar to real time date obtained by experiments. The depth of carters in numerical simulation is similar to experimental values. Figure 6.8, 6.13 and 6.18 shows simulation progression of bullet through different types of perforation. The graph of internal energy and kinetic energy shows that kinetic energy declines rapidly and internal energy upsurges. The kinetic energy of 7.62 x 51 mm armor piercing projectile is absorbed by the high hardness perforated steel

plate. This reduces effect of projectile on aluminum base armor plate. The kinetic energy of bullet keeps on reducing until velocity of bullet becomes zero. After failure of high hardness perforated armor plate, a small amount of kinetic energy is still available in projectile. This kinetic energy causes a few millimeters penetration in aluminum base plate.

All three cases of perforation i.e., circular, diamond shaped and slot shaped, have stopped penetration of 7.62 x 51 mm armor piercing projectile. All give same mass effectiveness value against rolled homogeneous armor steel and aluminum AA5083-H116 armor plate. The high hardness steel plates with slot shaped perforation is lightest in weight but has equal strength for stopping penetration of 7.62 x 51 mm armor piercing projectile to that of high hardness perforated plate with circular and diamond shaped perforations.

REFERENCES

[1] Y. Tarsi, D. Ben-Moshe, and G. Rosenberg, "An armour assembly for armoured vehicles," Patent EP 0 209 221 A1, 1986.

[2] R. A. Auyer, R. J. Buccellato, A. J. Gidynski, R. M. Ingersoll, and N. S. Sridharan, "Perforated Plate Armor," United States Patent 5,014,593, 1991.

[3] M. Ravid and Y. Hirschberg, "Ballistic Armor," United States Patent Patent US007513186B2, 2009.

[4] W. J. Norris and C. A. Smith, "Perforated Armor With Geometry Modified For Lighter Weight," Patent WO 2010/036411 A2, 2010.

[5] N. Kılıç, S. Bedir, A. Erdik, B. Ekici, A. Taşdemirci, and M. Güden, "Ballistic behavior of high hardness perforated armor plates against 7.62mm armor piercing projectile," *Materials & Design*, vol. 63, pp. 427-438, 2014/11/01/ 2014.

[6] R. C. Hibbeler, *Mechanics of Materials*, Tenth edition. ed. Pearson, 2015, pp. xvii, 877 pages.

[7] M. P. Groover, *Fundamentals of modern manufacturing : materials, processes, and systems*, 4th ed. Hoboken, NJ: J. Wiley & Sons, 2010, pp. xii, 1012 p.

[8] J. M. Gere and B. J. Goodno, *Mechanics of materials*, 8th ed. Stamford, CT: Cengage Learning, 2013, pp. xx, 1130 p.

[9] R. G. Budynas and J. K. Nisbett, *Shigley's Mechanical Engineering Design*, 9th ed. (McGraw-Hill series in mechanical engineering). New York: McGraw-Hill, 2011, pp. xxi, 1082 p.

[10] Y. Bai and B. Dodd, *Adiabatic shear localization : occurrence, theories and applications*. Oxford: Pergamon, 1992, pp. x, 378 p.

[11] M. Colakoglu, O. Soykasap, and T. Özek, "Experimental and Numerical Investigations on the Ballistic Performance of Polymer Matrix Composites Used in Armor Design," *Applied Composite Materials*, vol. 14, no. 1, pp. 47-58, 2007/01/01 2007.

[12] H. A. Sung, K. J. Woo, and J. K. Hee, "Development Trends of Ceramic Composite Armors for Combat Vehicles," *Journal of the Korean Society of Precision Engineering*, vol. 22, 2005.

[13] B. Basaran, "Computational Analysis of Advanced Composite Armor Systems," Master of Science in Mechanical Engineering, Mechanical Engineering, Middle East Technical University, 2007.

[14] T. Z. Blazynski, *Materials at high strain rates*. USA: Elsevier Applied Science, 1987, pp. xii, 302 p.

[15] P. G. Karandikar, G. Evans, S. Wong, M. K. Aghajanian, and M. Sennett, "A review of ceramics for armor applications," in *Advances in Ceramic Armor*, Florida United States, 2009, vol. 29, no. 6, pp. 163-175: John Wiley & Sons Inc.

[16] H. H. Warden, "Improved Ships Armor Plates," United States Patent 34539, 1862.

[17] *Military Specification: Armor Plate, Steel, Wrought, Homogeneous (for use in Combat-vehicles and for Ammunition Testing)*, MIL-A-12560H, 1984.

[18] T. J. Holmquist, A. M. Rajendran, D. W. Templeton, and K. D. Bishnoi, "A Ceramic Armor Material Database," U.S. Army Tank Automotive Research, Development and Engineering Center, United States13754, 1999.

[19] R. F. Ashton and D. S. Thompson, "Aluminum Armor Plate System," United States Patent 4,469,537, 1984.

[20] V. S. G. Murray, M. R. Bailey, and B. G. Spratt, "Depleted Uranium: A New Battlefield Hazard," *The Lancet*, vol. 360, pp. s31-s32, 2002.

[21] R. L. Cook, "Hard Faced Plastic Armor," United States Patent 3516898, 1966.

[22] J. S. Montgomery and M. G. H. Wells, "Titanium Armor Applications in Combat Vehicles," *JOM*, vol. 53, no. 4, pp. 29-32, 2001.

[23] P. J. Hogg, "Composites in Armor," *Science*, vol. 314, no. 5802, pp. 1100-1101, 2006.

[24] M. G. Cottrell, J. Yu, and D. R. J. Owen, "The adaptive and erosive numerical modelling of confined boron carbide subjected to large-scale dynamic loadings with element conversion to undeformable meshless particles," *International Journal of Impact Engineering*, vol. 28, no. 9, pp. 1017-1035, 2003.

[25] T. Børvik, O. S. Hopperstad, T. Berstad, and M. Langseth, "A computational model of viscoplasticity and ductile damage for impact and penetration," *European Journal of Mechanics - A/Solids*, vol. 20, no. 5, pp. 685-712, 2001.

[26] M. M. Nazeer, M. A. Khan, A. Naeem, and A.-u. Haq, "Analysis of conical tool perforation of ductile metal sheets," *International Journal of Mechanical Sciences,* vol. 42, no. 7, pp. 1391-1403, 2000.

[27] D. Liu and W. J. Stronge, "Ballistic limit of metal plates struck by blunt deformable missiles: experiments," *International Journal of Solids and Structures,* vol. 37, no. 10, pp. 1403-1423, 2000.

[28] A. Rusinek, J. A. Rodríguez-Martínez, R. Zaera, J. R. Klepaczko, A. Arias, and C. Sauvelet, "Experimental and numerical study on the perforation process of mild steel sheets subjected to perpendicular impact by hemispherical projectiles," *International Journal of Impact Engineering,* vol. 36, no. 4, pp. 565-587, 2009.

[29] M. A. G. Silva, C. Cismaşiu, and C. G. Chiorean, "Numerical simulation of ballistic impact on composite laminates," *International Journal of Impact Engineering,* vol. 31, no. 3, pp. 289-306, 2005.

[30] L. J. Deka, S. D. Bartus, and U. K. Vaidya, "Damage evolution and energy absorption of E-glass/polypropylene laminates subjected to ballistic impact," *Journal of Materials Science,* vol. 43, no. 13, pp. 4399-4410, 2008.

[31] L. J. Deka, S. D. Bartus, and U. K. Vaidya, "Multi-site impact response of S2-glass/epoxy composite laminates," *Composites Science and Technology,* vol. 69, no. 6, pp. 725-735, 2009.

[32] B. Wang, G. Lu, and M. K. Lim, "Experimental and numerical analysis of the response of aluminium oxide tiles to impact loading," *Journal of Materials Processing Technology,* vol. 51, no. 1-4, pp. 321-345, 1995.

[33] M. Lee and Y. H. Yoo, "Analysis of ceramic/metal armour systems," *International Journal of Impact Engineering,* vol. 25, no. 9, pp. 819-829, 2001.

[34] H. D. Espinosa, S. Dwivedi, P. D. Zavattieri, and G. Yuan, "A numerical investigation of penetration in multilayered material/structure systems," *International Journal of Solids and Structures,* vol. 35, no. 22, pp. 2975-3001, 1998.

[35] A. H. Sheikh, P. H. Bull, and J. A. Kepler, "Behaviour of multiple composite plates subjected to ballistic impact," *Composites Science and Technology,* vol. 69, no. 6, pp. 704-710, 2009.

[36] V. B. C. Tan, V. P. W. Shim, and T. E. Tay, "Experimental and numerical study of the response of flexible laminates to impact loading," *International Journal of Solids and Structures,* vol. 40, no. 23, pp. 6245-6266, 2003.

[37] V. S. Galvez and F. G. Diaz-Rubio, "Ballistic Impact On Ceramic/Composite Armours," *WIT Transactions on The Built Environment,* vol. 35, pp. 673-681, 1998.

[38] R. Cortés, C. Navarro, M. A. Martínez, J. Rodríguez, and V. Sanchez-Galvez, "Numerical modelling of normal impact on ceramic composite armours," *International Journal of Impact Engineering,* vol. 12, no. 4, pp. 639-650, 1992.

[39] I. S. Chocron Benloulo and V. Sánchez-Gálvez, "A new analytical model to simulate impact onto ceramic/composite armors," *International Journal of Impact Engineering,* vol. 21, no. 6, pp. 461-471, 1998.

[40] S. Sadanandan and J. G. Hetherington, "Characterisation of ceramic/steel and ceramic/aluminium armours subjected to oblique impact," *International Journal of Impact Engineering,* vol. 19, no. 9-10, pp. 811-819, 1997.

[41] J. G. Hetherington and P. F. Lemieux, "The effect of obliquity on the ballistic performance of two component composite armours," *International Journal of Impact Engineering,* vol. 15, no. 2, pp. 131-137, 1994.

[42] E. Dörre and H. Hübner, *Alumina : Processing, Properties, and Applications* (Materials research and engineering). Berlin ; New York: Springer-Verlag, 1984, pp. xiii, 329 p.

[43] B. Z. Haque, M. M. Kearney, and J. W. Gillespie Jr, "Advances in Protective Personnel and Vehicle Armors," *Recent Patents on Materials Sciencee,* vol. 5, no. 2, pp. 105-136, 2012.

[44] V. Madhu and T. B. Bhat, "Armour Protection and Affordable Protection for Futuristic Combat Vehicles," *Defence Science Journal,* vol. 61, no. 4, pp. 394-402, 2011.

[45] S. Balos, V. Grabulov, L. Sidjanin, M. Pantic, and I. Radisavljevic, "Geometry, mechanical properties and mounting of perforated plates for ballistic application," *Materials & Design,* vol. 31, no. 6, pp. 2916-2924, 2010.

[46] I. Radisavljevic, S. Balos, M. Nikacevic, and L. Sidjanin, "Optimization of geometrical characteristics of perforated plates," *Materials & Design,* vol. 49, pp. 81-89, 2013.

[47] B. Mishra, B. Ramakrishna, P. K. Jena, K. Siva Kumar, V. Madhu, and N. K. Gupta, "Experimental studies on the effect of size and shape of holes on damage and

microstructure of high hardness armour steel plates under ballistic impact," *Materials & Design*, vol. 43, pp. 17-24, 2013.

[48] B. Mishra, P. K. Jena, B. Ramakrishna, V. Madhu, T. B. Bhat, and N. K. Gupta, "Effect of tempering temperature, plate thickness and presence of holes on ballistic impact behavior and ASB formation of a high strength steel," *International Journal of Impact Engineering*, vol. 44, pp. 17-28, 2012.

[49] R. A. Howell, J. Montgomery, and D. C. Van Aken, "Advancements in steel for weight reduction of P900 armor plate," Army Research Lab Aberdeen Proving Ground Md Survivability Materials Branch 2008.

[50] S. Chocron, C. E. Anderson, D. J. Grosch, and C. H. Popelar, "Impact of the 7.62-mm APM2 projectile against the edge of a metallic target," *International Journal of Impact Engineering*, vol. 25, no. 5, pp. 423-437, 2001.

[51] Z. Rosenberg and E. Dekel, *Terminal Ballistics*. 2016.

[52] Z. Rosenberg, Y. Ashuach, Y. Yeshurun, and E. Dekel, "On the main mechanisms for defeating AP projectiles, long rods and shaped charge jets," *International Journal of Impact Engineering*, vol. 36, no. 4, pp. 588-596, 2009.

[53] *SIMULIA Abaqus CAE User Assistance 2018*. Dassault Systèmes, 2018.

[54] *ANSYS AUTODYN SPH User Manual & Tutorial Version 4.3*. Century Dynamics Inc., 2005.

[55] *MSC Dytran 2008 User's Guide*. United States: MSC Software Corporation, 2008.

[56] T. Børvik, M. Langseth, O. S. Hopperstad, and K. A. Malo, "Ballistic penetration of steel plates," *International Journal of Impact Engineering*, vol. 22, no. 9-10, pp. 855-886, 1999.

[57] J. Buchar, J. Voldrich, S. Rolc, and J. Lisy, "Ballistic performance of dual hardness armor," presented at the 20th International symposium on Ballistics, Orlando, 2002.

[58] T. Børvik, O. S. Hopperstad, T. Berstad, and M. Langseth, "Perforation of 12mm thick steel plates by 20mm diameter projectiles with flat, hemispherical and conical noses," *International Journal of Impact Engineering*, vol. 27, no. 1, pp. 37-64, 2002.

[59] S. Dey, T. Børvik, X. Teng, T. Wierzbicki, and O. S. Hopperstad, "On the ballistic resistance of double-layered steel plates: An experimental and numerical investigation," *International Journal of Solids and Structures*, vol. 44, no. 20, pp. 6701-6723, 2007.

[60] X. Teng, T. Wierzbicki, and M. Huang, "Ballistic resistance of double-layered armor plates," *International Journal of Impact Engineering*, vol. 35, no. 8, pp. 870-884, 2008.

[61] T. Børvik, S. Dey, and A. H. Clausen, "Perforation resistance of five different high-strength steel plates subjected to small-arms projectiles," *International Journal of Impact Engineering*, vol. 36, no. 7, pp. 948-964, 2009.

[62] D. S. Preece and V. S. Berg, "Bullet Impact on Steel and Kevlar®/Steel Armor: Computer Modeling and Experimental Data," presented at the Problems Involving Thermal Hydraulics, Liquid Sloshing, and Extreme Loads on Structures, 2004.

[63] D. L. Orphal, R. R. Franzen, A. J. Piekutowski, and M. J. Forrestal, "Penetration of confined aluminum nitride targets by tungsten long rods at 1.5–4.5 km/s," *International Journal of Impact Engineering*, vol. 18, no. 4, pp. 355-368, 1996.

[64] C. E. Anderson, V. Hohler, J. D. Walker, and A. J. Stilp, "Time-resolved penetration of long rods into steel targets," *International Journal of Impact Engineering*, vol. 16, no. 1, pp. 1-18, 1995.

[65] A. A. Almohandes, M. S. Abdel-Kader, and A. M. Eleiche, "Experimental investigation of the ballistic resistance of steel-fiberglass reinforced polyester laminated plates," *Composites Part B: Engineering*, vol. 27, no. 5, pp. 447-458, 1996/01/01/ 1996.

[66] M. J. Thali, B. P. Kneubuehl, U. Zollinger, and R. Dirnhofer, "A high-speed study of the dynamic bullet–body interactions produced by grazing gunshots with full metal jacketed and lead projectiles," *Forensic Science International*, vol. 132, no. 2, pp. 93-98, 2003.

[67] H. M. Hsiao and I. M. Daniel, "Strain rate behavior of composite materials," *Composites Part B: Engineering*, vol. 29, no. 5, pp. 521-533, 1998.

[68] B. Hopkinson, "X. A method of measuring the pressure produced in the detonation of high, explosives or by the impact of bullets," *Philosophical Transactions of the Royal Society of London. Series A, Containing Papers of a Mathematical or Physical Character*, vol. 213, no. 497-508, pp. 437-456, 1914.

[69] M. A. Kaiser, "Advancements in the Split Hopkinson Bar Test," Master of Science, Mechanical Engineering, Virginia Polytechnic Institute and State University, Virginia 1998.

[70] H. Kolsky, "An Investigation of the Mechanical Properties of Materials at very High Rates of Loading," *Proceedings of the Physical Society. Section B,* vol. 62, no. 11, pp. 676-700, 1949.

[71] P. Verleysen and J. Degrieck, "A modified digital phase-shift moiré technique for impact deformation measurements," *Optics and Lasers in Engineering,* vol. 42, no. 6, pp. 653-671, 2004.

[72] H. Zhao, "Material behaviour characterisation using SHPB techniques, tests and simulations," *Computers & Structures,* vol. 81, no. 12, pp. 1301-1310, 2003.

[73] P. Verleysen and J. Degrieck, "Experimental investigation of the deformation of Hopkinson bar specimens," *International Journal of Impact Engineering,* vol. 30, no. 3, pp. 239-253, 2004.

[74] N. Kılıç and B. Ekici, "Ballistic resistance of high hardness armor steels against 7.62mm armor piercing ammunition," *Materials & Design,* vol. 44, pp. 35-48, 2013.

[75] X. Quan and N. Birnbaum, "SPH Simulation of the Ballistic Perforation of GFRP," in *Proceedings of the 18th International Symposium on Ballistics,* 1999, pp. 15-19.

[76] G. R. Johnson and W. H. Cook, "A constitutive model and data for metals subjected to large strains, high strain rates and high temperatures," in *Proceedings of the 7th International Symposium on Ballistics,* 1983, vol. 21, no. 1, pp. 541-547.

[77] A. Abbasi-Bani, A. Zarei-Hanzaki, M. H. Pishbin, and N. Haghdadi, "A comparative study on the capability of Johnson–Cook and Arrhenius-type constitutive equations to describe the flow behavior of Mg–6Al–1Zn alloy," *Mechanics of Materials,* vol. 71, pp. 52-61, 2014.

[78] M. Murugesan and D. Jung, "Johnson Cook Material and Failure Model Parameters Estimation of AISI-1045 Medium Carbon Steel for Metal Forming Applications," *Materials,* vol. 12, no. 4, 2019.

[79] M. Murugesan, S. Lee, D. Kim, Y.-H. Kang, and N. Kim, "A Comparative Study of Ductile Damage Models Approaches for Joint Strength Prediction in Hot Shear Joining Process," *Procedia Engineering,* vol. 207, pp. 1689-1694, 2017.

[80] S. Hiermaier, *Structures under crash and impact : continuum mechanics, discretization and experimental characterization*. New York: Springer, 2008, pp. xii, 410 p.

[81] Z. Rosenberg and E. Dekel, "Revisiting the perforation of ductile plates by sharp-nosed rigid projectiles," *International Journal of Solids and Structures*, vol. 47, no. 22, pp. 3022-3033, 2010/11/01/ 2010.

[82] R. Woodward, "Materials for projectile disruption," in *Materials Forum*, 1988, vol. 12, pp. 26-30.

[83] K. Frank, "Armor-Penetrator Performance Measures," US Army Ballistic Research Laboratory1981.

[84] *Military Specifications Armor Plate, Aluminum Alloy, Weldable 5083 and 5456*, 1984.